Available online at www.sciencedirect.com
SCIENCE DIRECT®
Journal of Computational Physics 198 (2004) 80–105
JOURNAL OF COMPUTATIONAL PHYSICS
www.elsevier.com/locate/jcp

A Godunov-type method in Lagrangian coordinates for computing linearly-perturbed planar-symmetric flows of gas dynamics

Jean-Marie Clarisse [a], Stéphane Jaouen [a,*], Pierre-Arnaud Raviart [b]

[a] *CEA Bruyères le Châtel, B.P. 12, 91680 Bruyères le Châtel, France*
[b] *Laboratoire Jacques-Louis Lions, 4 Place Jussieu, Université Pierre et Marie Curie, 75252 Paris CEDEX 05, France*

Received 4 February 2003; received in revised form 21 November 2003; accepted 5 January 2004
Available online 10 February 2004

Abstract

Linear stability studies of complex flows require that efficient numerical methods be devised for predicting growth rates of multi-dimensional perturbations. For one-dimensional (1D) basic flows – i.e. of planar, cylindrical or spherical symmetry – a general numerical approach is viable which consists in solving simultaneously the one-dimensional equations of gas dynamics and their linearized forms for three-dimensional perturbations. Extensions of artificial viscosity methods have thus been used in the past. More recently [Equations aux dérivées partielles et applications, articles dédiés à J.-L. Lions, 1998], Godunov-type schemes for single-fluid flows of gas dynamics and magnetohydrodynamics have been proposed. Pursuing this effort, we introduce, within the Lagrangian perturbation approach, a class of Godunov-type schemes which is well suited for solving multi-material problems of gas dynamics. These schemes are developed here for the planar-symmetric case and comprise two second-order extensions. The numerical capabilities of these methods are illustrated by computations of Richtmyer–Meshkov instabilities occurring at a single material interface. A systematic comparison of numerically computed growth rates with results of the linear theory for the Richtmyer–Meshkov instability is provided.

Keywords: Gas dynamics; Linearized stability in Lagrangian coordinates; Richtmyer–Meshkov instability; Godunov-type methods

1. Introduction

Many problems in fluid mechanics and in physics lead to stability studies of complex flows. Most often, such stability studies cannot be performed analytically and must be investigated numerically. In any case, an essential preliminary step consists in performing a linear stability analysis of the basic flow under study. Hence, there is a demand for devising efficient numerical methods for predicting linear perturbation evo-

* Corresponding author. Tel.: +33-1-69-26-68-48; fax: +33-1-69-26-70-93.
E-mail addresses: jean-marie.clarisse@cea.fr (J.-M. Clarisse), stephane.jaouen@cea.fr (S. Jaouen), pa@raviart.com (P.-A. Raviart).

0021-9991/$ - see front matter
doi:10.1016/j.jcp.2004.01.003

lutions in complex flows. Fortunately, in some situations – such as those found in inertial confinement fusion (ICF), our primary motivation here – the basic flow is one-dimensional – i.e. planar, cylindrically or spherically symmetric – so that the linearized stability problem reduces to computing multi-dimensional linear perturbations about a 1D flow. This task may be achieved in a fairly inexpensive, reliable and accurate way by using 1D numerical codes for computing simultaneously the basic flow and the modal (Fourier, in planar symmetry) components of its linear perturbations. The underlying fluid code may either be Eulerian or Lagrangian. Here we shall focus on the linear Lagrangian perturbation approach which appears to be well suited for studying the linear hydrodynamic stability of ICF pellets, and restrict ourselves, for the sake of simplicity, to the case of 1D planar-symmetric basic flows. The case of 1D spherically-symmetric basic flows will be addressed in a subsequent paper.

This linear perturbation computation approach offers decisive advantages over 2D or 3D computations. First of all, given the computational grid coarseness commonly advised for obtaining "accurate" 2D calculations of hydrodynamic instabilities (e.g. see [19]), the computational burden needed for solving the one-dimensional equations for the basic flow and its perturbations is, at least, two (respectively four) orders of magnitude lower than that required by standard 2D (resp. 3D) methods. Thanks to this reduced computational cost, "converged" results of linear stability problems for complex flows may be produced in a very efficient manner. Hence, for instance, detailed and accurate descriptions of the spatial structures and time evolutions of perturbations in a planar ablation flow – in the so-called "ablative Richtmyer–Meshkov instability" configuration [16] – have been obtained for a wide range of perturbation wavenumbers [4]. Such results, corroborating in part the qualitative analysis of [16], are yet to be produced by means of 2D computations. Indeed, obtaining the same quality of data from 2D/3D simulations would be a tedious and cumbersome task. This efficiency – unmatched by 2D/3D computations – is especially needed in ICF applications where one is interested in obtaining detailed linear responses – both in time and space – of complex implosion flows for a wide range of initial and boundary condition perturbations. Furthermore, computing linear perturbations avoids the accuracy limitations faced by 2D/3D computations when dealing with perturbations of small relative amplitudes – a situation inherent to linear stability analyses.

These features have been previously exploited in numerous linear stability analyses of unsteady flows, whether in gas dynamics [6,17], astrophysics [7], or in the more specific context of ICF [10,18,24,31]. When dealing with shock waves, these earlier works relied on artificial viscosity methods under the form of appropriate linearizations of the classical scheme of von Neumann and Richtmyer [30]. More recently, this linear perturbation computation approach has been reconsidered within the framework of nonlinear hyperbolic systems of conservation laws [11,12,14,28]. In particular, Godunov-type schemes based on a linearization of the Roe method in Lagrangian coordinates [27] have been proposed and have produced convincing results for single fluid flows of gas dynamics and of magnetohydrodynamics [28]. Here, we pursue this effort having in mind applications to linear stability analyses of shocked material discontinuities in multi-material flows. Following the analysis by Després [9] of Lagrangian systems of conservation laws, we propose a class of Godunov-type schemes for computing simultaneously the basic and the linearized flows. Using an approximate Riemann solver due to Després [9], these schemes are well suited for handling multi-material problems of gas dynamics [20]. As an illustration of the scheme numerical capabilities we have chosen to consider the simple, yet demanding, configuration of the Richtmyer–Meshkov instability [25,29] for a single material interface separating perfect gases of different adiabatic exponents. (Note that this kind of configurations had already been treated with an artificial viscosity method in [17] and more recently [13] with the linearized Roe method, the latter, however, dealing exclusively with gases of identical adiabatic exponents.) More complex flow configurations may equally be considered but are beyond the scope of this paper.

The plan of the present paper is as follows. In Section 2, we introduce, under the assumptions of gas dynamics, the linearized Cauchy problems for stability analyses in terms of Lagrangian perturbations. In particular, the set of linearized equations are fully derived with the help of a Helmholtz decomposition of

the transverse linear motion (Appendix B), and initial conditions for geometrically perturbed material interfaces are discussed (Appendix C). In Section 3, we introduce the present class of Godunov-type schemes including second-order extensions of these methods. Section 4 presents the numerical application of these schemes to the Richtmyer–Meshkov instability which occurs at a single material interface between two different perfect gases. A systematic quantitative comparison of the numerically computed growth rates with results found in the literature [34,35] is carried out for various incident shock strengths, initial fluid density ratios and adiabatic exponent pairs.

2. Linearized Cauchy problems for stability analyses in Lagrangian perturbations

Consider the motion of an inviscid, non-heat-conducting fluid, obeying an arbitrary equation of state. Given a cartesian coordinate system (x_1, x_2, x_3) of orthonormal vector basis $(\mathbf{e}_1, \mathbf{e}_2, \mathbf{e}_3)$, and a Lagrangian coordinate system (ξ_1, ξ_2, ξ_3), the equations of a fluid particle trajectory $t \mapsto \mathbf{x}(\boldsymbol{\xi}, t)$ read

$$\frac{\partial \mathbf{x}}{\partial t}(\boldsymbol{\xi}, t) = \mathbf{u}(\boldsymbol{\xi}, t), \tag{1}$$

where $\mathbf{u}(= u_j \mathbf{e}_j)$ denotes the particle velocity. (Herein summation over a repeated subscript is always implied.) For any function φ of the variables $(\boldsymbol{\xi}, t)$, we use the notation $\bar{\varphi}$ to designate the function of $(\mathbf{x}, t)$ defined by

$$\bar{\varphi}(\mathbf{x}(\boldsymbol{\xi}, t), t) \stackrel{\text{def}}{=} \varphi(\boldsymbol{\xi}, t).$$

With this convention, the Lagrangian form of the equations of motion – in the absence of external forces – comes as

$$\frac{\partial \mathbf{V}}{\partial t} + \tau \frac{\partial}{\partial x_j} \overline{\mathbf{G}_j(\mathbf{V})} = \mathbf{0}, \tag{2}$$

with

$$\mathbf{V} = \begin{pmatrix} \tau \\ \mathbf{u} \\ e \end{pmatrix}, \quad \mathbf{G}_j(\mathbf{V}) = \begin{pmatrix} -u_j \\ p\mathbf{e}_j \\ pu_j \end{pmatrix}, \quad 1 \leqslant j \leqslant 3, \tag{3}$$

where τ is the fluid specific volume, p the pressure and e the specific total energy. This system of equations is completed by the fluid equation of state, here under the form

$$p = P(\tau, \mathscr{E}), \tag{4}$$

giving the pressure of the fluid as a function of its specific volume and specific internal energy $\mathscr{E} = e - u_j u_j/2$. With these definitions, solutions to (2) take values in the set of states given by

$$\mathscr{V} = \left\{ \mathbf{V}; \tau > 0, \ \mathbf{u} \in \mathbb{R}^3, \ e - u_j u_j/2 > 0 \right\}.$$

Independently of Eq. (2), a first integral of the evolution equation for the fluid specific volume τ is provided by the conservation of mass written down for an infinitesimal fluid element. Letting

$$J(\boldsymbol{\xi}, t) = \det\left(\frac{\partial x_i}{\partial \xi_j}(\boldsymbol{\xi}, t) \right) \tag{5}$$

denote the Jacobian of the transformation $\boldsymbol{\xi} \mapsto \mathbf{x}$, this first integral taken at the point $\boldsymbol{\xi}$ may be written as

$$\rho(\boldsymbol{\xi},t)J(\boldsymbol{\xi},t)=\rho_{\star}(\boldsymbol{\xi}), \tag{6}$$

where $\rho_{\star}$ stands for the fluid density in some reference state – possibly virtual – of the fluid for which $J(\boldsymbol{\xi})=1$.

Given a real positive constant T we consider, in the following, Cauchy problems (initial value problems – IVPs) of the kind:

Find a pair of functions $(\mathbf{V},\mathbf{x}):(\boldsymbol{\xi},t)\in\mathbb{R}^3\times(0,T)\mapsto(\mathbf{V},\mathbf{x})(\boldsymbol{\xi},t)\in\mathscr{V}\times\mathbb{R}^3$ solution of

$$\begin{cases}\frac{\partial\mathbf{V}}{\partial t}+\tau\frac{\partial}{\partial x_j}\overline{\mathbf{G}_j(\mathbf{V})}=\mathbf{0}, \quad \frac{\partial\mathbf{x}}{\partial t}=\mathbf{u}, \quad (\boldsymbol{\xi},t)\in\mathbb{R}^3\times(0,T),\\ (\mathbf{V},\mathbf{x})(\boldsymbol{\xi},0)=(\mathbf{V}_0,\mathbf{x}_0)(\boldsymbol{\xi}), \quad \boldsymbol{\xi}\in\mathbb{R}^3,\end{cases} \tag{7}$$

where the initial data $(\mathbf{V}_0,\mathbf{x}_0)$ are a priori arbitrary.

As is well known, such IVPs may be ill-posed in the class of $\mathscr{C}^1$ functions defined in $\mathbb{R}^3\times(0,T)$ and weak solutions, when they exist, are to be sought as piecewise smooth distributions over $\mathbb{R}^3\times(0,T)$. When studying a solution, say $\mathbf{V}^0$, of such an IVP, the question of its stability with respect to perturbations of its initial data $\mathbf{V}_0^0$ is one that naturally arises in many problems of fluid mechanics.

Such a stability problem may be conveniently formulated in terms of a perturbation parameter, say $\varepsilon\in\mathbb{R}$, as follows. Let $\mathbf{V}_0(\boldsymbol{\xi};\varepsilon)$ denote the perturbed initial data, and let ε be chosen so that for $\varepsilon=0$ we have:

$$\mathbf{V}_0(\boldsymbol{\xi};0)=\mathbf{V}_0^0(\boldsymbol{\xi}), \quad \forall\boldsymbol{\xi}\in\mathbb{R}^3,$$

where $\mathbf{V}_0^0(\boldsymbol{\xi})$ is the initial value of the IVP (7) satisfied by $\mathbf{V}^0$, which, from now on, will be referred to as the *basic solution*. Substituting these perturbed initial data in (7) thus define perturbed IVPs whose solutions are denoted by $\mathbf{V}(\cdot,\cdot;\varepsilon)$. One then assumes that there exists a non-empty neighborhood of $\varepsilon=0$, say $\mathscr{I}_0$, such that for any ε in $\mathscr{I}_0$ the corresponding IVP admits a solution. A stability analysis of the basic solution consists then in studying how the solutions $\mathbf{V}(\cdot,\cdot;\varepsilon)$ depart in space and time from $\mathbf{V}^0$ as ε spans $\mathscr{I}_0$.

In the absence of further assumptions about the nature of the basic solution – e.g. regarding its steadiness, periodicity, etc. – one is compelled to solve the IVPs for $\mathbf{V}(\cdot,\cdot;\varepsilon)$ in the independent variables $(\boldsymbol{\xi},t)$. Furthermore when various initial values for the basic problem (7) have to be considered – as it is the case here – one has no other choice but to have recourse to numerical approximation methods for handling such problems. However in the limit of vanishing ε – i.e. for infinitesimal perturbations – the stability problem for the basic solution may be linearized, in which case the set of perturbed IVPs given by ε spanning $\mathscr{I}_0$, is replaced by a single IVP for *linear perturbations*.

Various formulations of this IVP may be obtained depending on the definition of the linear perturbations that is retained: e.g. Eulerian or Lagrangian. Here we choose to adopt the Lagrangian perturbation approach [2,22] which has been previously used for various problems of gas dynamics [6,17] and ICF [10,24,31]. This choice is motivated by the fact that relying on Lagrangian perturbations greatly simplifies, both at the theoretical and computational levels, the handling of geometrically perturbed material discontinuities. We note that the method developed in [11–14,28] which is also based on a formulation of the linear perturbation equations in Lagrangian coordinates, differs however, in general, from the Lagrangian perturbation approach.

2.1. The linearized problem for Lagrangian perturbations

2.1.1. Principles of Lagrangian perturbations

Let us recall that a Lagrangian perturbation of a given fluid quantity φ amounts to considering, for a fluid particle M, the difference

$$\delta\varphi_{\mathrm{M}}(t;\varepsilon)=\varphi_{\mathrm{M}}(t;\varepsilon)-\varphi_{\mathrm{M}}(t;0)=\varphi(\boldsymbol{\xi}_{\mathrm{M}},t;\varepsilon)-\varphi(\boldsymbol{\xi}_{\mathrm{M}},t;0),$$

cf. [2,22]. As is obvious, retaining a formulation in terms of Lagrangian perturbations implicitly requires that the set of fluid particles which is considered, say $\mathscr{D}$, remains the same whatever t in $(0,T)$ and ε in $\mathscr{I}_0$. Equivalently, any material quantity which is a function of the fluid particles – e.g. mass, particle Lagrangian coordinates – must be conserved in $\mathscr{D}$ as (t,ε) spans $(0,T)\times\mathscr{I}_0$. Consequently a coordinate system, say (ξ_1,ξ_2,ξ_3), candidate for formulating the Lagrangian perturbation equations must be such that:

1. The coordinate system (ξ_1,ξ_2,ξ_3) is a Lagrangian system of coordinates for the fluid particles of $\mathscr{D}$, during their motion in time *and* as ε spans $\mathscr{I}_0$.
2. For any (t,ε) in $(0,T)\times\mathscr{I}_0$, the transformation $\mathbf{x}\mapsto\boldsymbol{\xi}$ defines, almost everywhere in $\mathbb{R}^3$, a diffeomorphism of $\mathbb{R}^3$.

A direct consequence of the first of these two requirements is that the first integral (6) holds at any point $(\boldsymbol{\xi},t,\varepsilon)$ of $\mathbb{R}^3\times(0,T)\times\mathscr{I}_0$ for which the transformation $\boldsymbol{\xi}\mapsto\mathbf{x}$ is a diffeomorphism, i.e. we have

$$\rho(\boldsymbol{\xi},t;\varepsilon)J(\boldsymbol{\xi},t;\varepsilon)=\rho_\star(\boldsymbol{\xi}). \tag{8}$$

Following [17], we define *formally*, for any integer n, a nth-order Lagrangian perturbation operator $\mathrm{d}^n(\cdot)$ as

$$\mathrm{d}^n:\varphi(\cdot,\cdot;\varepsilon)\mapsto\mathrm{d}^n\varphi(\cdot,\cdot)=\left(\frac{\partial^n\varphi}{\partial\varepsilon^n}(\cdot,\cdot;\varepsilon)\right)\Bigg|_{\varepsilon=0}. \tag{9}$$

The linear Lagrangian perturbation of φ is then simply defined as $\mathrm{d}^1\varphi$ while the basic solution φ^0 corresponds to $\mathrm{d}^0\varphi$. When applying $\mathrm{d}^n(\cdot)$ to any function of some arguments, the variables ξ_1, ξ_2, ξ_3, t and ε must be considered as independent variables, all other variables being taken as dependent. Hence, in particular, the operator $\mathrm{d}^n(\cdot)$ commutes with any partial differentiation with respect to the Lagrangian coordinates ξ_j, $1\leqslant j\leqslant 3$, or t. That is all there is to know in order to derive the equations for the linear Lagrangian perturbations of the basic solution.

2.1.2. Conservation laws for linear Lagrangian perturbations

Within the formalism introduced in the previous paragraph, the linearization of the perturbed IVPs deduced from (7) is carried out formally by applying the operator $\mathrm{d}^1(\cdot)$ to each of the equations therein.

Applying this operator to initial values is straightforward while the linear Lagrangian perturbation of the trajectory equation (1) comes down to

$$\frac{\partial\mathrm{d}^1\mathbf{x}}{\partial t}=\mathrm{d}^1\mathbf{u}. \tag{10}$$

Concerning the first integral (8), we infer from Proposition 1 of Appendix A that

$$\mathrm{d}^1\tau=\tau^0\frac{\partial\mathrm{d}^1x_j}{\partial\xi_k}\mathrm{d}^0\left(\frac{\partial\xi_k}{\partial x_j}\right), \tag{11}$$

which is in fact nothing else but Eq. 12 of ([2], Chapter VII). Using this result and Proposition 2 of Appendix A, the linear Lagrangian perturbation of Eq. (2) comes readily as the following system of conservation laws:

$$\frac{\partial\mathrm{d}^1\mathbf{V}}{\partial t}+\tau^0\left\{\frac{\partial}{\partial\xi_k}\mathrm{d}^1\mathbf{G}_j(\mathbf{V})+\frac{\partial}{\partial\xi_k}\mathbf{G}_j(\mathbf{V}^0)\frac{\partial\mathrm{d}^1x_l}{\partial\xi_m}\mathrm{d}^0\left(\frac{\partial\xi_m}{\partial x_l}\right)-\frac{\partial}{\partial\xi_m}\mathbf{G}_j(\mathbf{V}^0)\mathrm{d}^0\left(\frac{\partial\xi_m}{\partial x_l}\right)\frac{\partial\mathrm{d}^1x_l}{\partial\xi_k}\right\}\mathrm{d}^0\left(\frac{\partial\xi_k}{\partial x_j}\right)=\mathbf{0}, \tag{12}$$

with, for the definitions of the flux component linear perturbations,

$$\mathrm{d}^1\mathbf{G}_j(\mathbf{V})=\frac{\mathrm{d}\mathbf{G}_j}{\mathrm{d}\mathbf{V}}(\mathbf{V}^0)\mathrm{d}^1\mathbf{V},\quad 1\leqslant j\leqslant 3, \tag{13}$$

where $d\mathbf{G}_j/d\mathbf{V}$ denotes the Jacobian matrix of $\mathbf{G}_j(\mathbf{V})$, $1 \leqslant j \leqslant 3$. This system is completed by the linearized form of the equation of state (4), or

$$d^1 p = P_\tau(\tau^0, \mathscr{E}^0) d^1\tau + P_{\mathscr{E}}(\tau^0, \mathscr{E}^0) d^1\mathscr{E}, \tag{14}$$

with $d^1\mathscr{E} = d^1 e - u_j^0 d^1 u_j$. In this relation, the notations P_τ and $P_{\mathscr{E}}$ refer to the thermodynamical partial derivatives $(\partial P/\partial\tau)_{\mathscr{E}}$ and $(\partial P/\partial\mathscr{E})_\tau$, respectively.

The above linearization procedure makes sense if $\mathbf{V}^0$ is a smooth enough basic solution. When this is not the case – as when $\mathbf{V}^0$ presents a material discontinuity or a shock front – Eq. (12) is a first-order linear system for $d^1\mathbf{V}$ with *discontinuous* coefficients. Regardless of the smoothness of the initial data $d^1\mathbf{V}_0$, the Cauchy problem associated to (12) is in general ill-posed in the class of functions. In fact solutions must be sought in a class of *measures*: see [3,11]. Such peculiarities are of course due to the choice of a general approach in solving the above IVPs. An alternative approach, which is classical in fluid mechanics, consists in isolating the discontinuities of the basic solution and use the corresponding jump relations as boundary conditions for the perturbations (e.g. see [23,35]). However in the present context, this approach would imply keeping track of an arbitrary number of discontinuities as the basic solution evolves in time, a task which could rapidly become intractable in practice. On the other hand material discontinuities, such as contact discontinuities separating immiscible fluids, are handled in a systematic and simple way due to the Lagrangian description of the linearized fluid motion. Indeed Godlewski et al. [12] have shown that in this case the solutions of the linearized Cauchy problems for a contact discontinuity of a single fluid belong to the class of functions rather than to a class of measures.

2.2. Particular case of one-dimensional motions in planar symmetry

We now turn to the particular situation which is of primary interest in this paper, namely the case of basic solutions corresponding to 1D motions with planar symmetry.

2.2.1. Definition of the Lagrangian coordinate system (ξ_1, ξ_2, ξ_3)

Having in mind the requirements (see Section 2.1) bearing on the Lagrangian coordinate system (ξ_1, ξ_2, ξ_3), and assuming that the x_1-axis coincides with the direction of the basic motion, we define, quite naturally, the coordinate ξ_1 to be such that

$$\xi_1 = \int \bar{\rho}^0(x_1, t) dx_1, \tag{15}$$

for all t in $(0, T)$, and choose ξ_2 and ξ_3 to be the constant coordinates in the x_2x_3-plane – or *transverse plane* – of the fluid particles in their basic flow motions. With this definition, Eqs. (1) and (2) satisfied by the basic solution $(\mathbf{V}^0, \mathbf{x}^0)$ reduce to the classical form of the one-dimensional gas dynamics equations written in Lagrangian coordinates, namely

$$\frac{\partial \mathbf{V}^0}{\partial t} + \frac{\partial}{\partial \xi_1}\mathbf{f}(\mathbf{V}^0) = \mathbf{0}, \tag{16a}$$

$$\frac{\partial x_1^0}{\partial t} = u_1^0, \tag{16b}$$

$$x_i^0 = \text{cst}, \quad i = 2, 3, \tag{16c}$$

with the notations

$$\mathbf{V} = \begin{pmatrix} \tau \\ u_1 \\ e \end{pmatrix}, \quad \mathbf{f}(\mathbf{V}) = \begin{pmatrix} -u_1 \\ p \\ pu_1 \end{pmatrix}. \tag{17}$$

The system of linear perturbation conservation laws (12) takes also a much simpler form, especially once a Helmholtz decomposition of the linearized motion in the transverse plane is performed: see Appendix B. Furthermore, the resulting 3D system of Eqs. (B.3), (B.4), (B.6) and (B.8) may then be reduced to a 1D system for the Fourier components – in the transverse plane – of the linear perturbations.

2.2.2. Transverse Fourier component equations

Indeed, introducing for any function $\mathrm{d}^1\varphi(\boldsymbol{\xi}, t)$ the notation

$$\hat{\varphi}(\xi_1, t; \mathbf{k}_\perp) = \int_{\mathbb{R}^2} \mathrm{d}^1\varphi(\boldsymbol{\xi}, t) \exp\{\mathrm{i}(k_2\xi_2 + k_3\xi_3)\}\mathrm{d}\xi_3\,\mathrm{d}\xi_2,$$

where $\mathbf{k}_\perp = k_2\mathbf{e}_2 + k_3\mathbf{e}_3$ is the transverse wavevector, the linear perturbation equations (10) and (12) are replaced by the (ξ_2, ξ_3)-Fourier transforms of Eqs. (B.3), (B.4), (B.6), (B.8) and (B.9), or

$$\frac{\partial\hat{\mathbf{V}}}{\partial t} + \frac{\partial}{\partial\xi_1}\left\{\frac{\mathrm{d}\mathbf{f}}{\mathrm{d}\mathbf{V}}(\mathbf{V}^0)\hat{\mathbf{V}}\right\} = -\frac{\partial}{\partial\xi_1}\mathbf{f}(\mathbf{V}^0)\hat{\Theta} + \tau^0\hat{\Omega}\begin{pmatrix} 1 \\ 0 \\ -p^0 \end{pmatrix}, \tag{18a}$$

$$\frac{\partial\hat{\Omega}}{\partial t} = k_\perp^2\left(\tau^0\hat{p} - \frac{\partial p^0}{\partial\xi_1}\widehat{x_1}\right), \tag{18b}$$

$$\frac{\partial\widehat{x_1}}{\partial t} = \widehat{u_1}, \tag{18c}$$

$$\frac{\partial\hat{\Theta}}{\partial t} = \hat{\Omega}, \tag{18d}$$

with: the definitions (17) for the vectors $\mathbf{V}^0$, $\hat{\mathbf{V}}$ and $\mathbf{f}$, the Fourier transforms of Eq. (B.7) for the transverse dilatation $\hat{\Theta}$ and expansion $\hat{\Omega}$, and the notation $k_\perp = \|\mathbf{k}_\perp\|$. Hence the linear perturbation transverse Fourier component equations consist in: (i) an inhomogeneous system of 1D linear conservation laws (18a), and (ii) time-differential equations (18b–d), the whole being supplemented by the Fourier transforms of the linearized equation of state (14), i.e.

$$\hat{p} = P_\tau(\tau^0, \mathscr{E}^0)\hat{\tau} + P_{\mathscr{E}}(\tau^0, \mathscr{E}^0)\hat{\mathscr{E}} \tag{19}$$

with $\hat{\mathscr{E}} = \hat{e} - u_1^0\widehat{u_1}$, and of the first integral (B.1) which reads

$$\hat{\tau} = \frac{\partial\widehat{x_1}}{\partial\xi_1} + \tau^0\hat{\Theta}. \tag{20}$$

As the transverse wavevector $\mathbf{k}_\perp$ only intervenes in (18)–(20) through its modulus, differences among Fourier components of identical wavenumbers but distinct wavevectors only result from differences in their respective initial and boundary conditions.

A broad range of initial conditions for the above equations may be considered. For multi-material flows, the case of geometrically perturbed material contact discontinuities is of crucial importance as these are prone to Rayleigh–Taylor and Richtmyer–Meshkov instabilities. The simplest configuration of a single

material interface between two immiscible fluids of arbitrary equations of state is addressed in Appendix C. In particular, it appears that initial conditions in this case may be chosen – within the Lagrangian perturbation approach – in the *class of functions* rather than – for the perturbation method of [13] – in a class of measures. This result turns out to be very useful in practical applications: see Section 4.

3. Numerical schemes

We propose in this section to derive numerical schemes for computing simultaneously the basic and the linearized flow solutions to (16) and (18). If a Godunov-type method for computing the linearized flow solutions has already been developed in [28], this method – based on a Roe solver – hardly applies in multimaterial problems, the difficulty lying in the definition of the Roe matrix at the interface between two different materials. Here, benefiting from the formalism described by Després in [9], we show how a Godunov-type method can be easily achieved in this case.

Herein, for simplicity, the subscript 1 relative to the longitudinal variables ($\xi = \xi_1$, $x = x_1$ and $u = u_1$) and the superscript 0 relative to the basic flow ($\mathbf{V} = \mathbf{V}^0$) have been removed.

3.1. Numerical schemes for the basic flow

In this section, we focus on the discretization of (16a) satisfied by $\mathbf{V}$, namely

$$\frac{\partial \mathbf{V}}{\partial t} + \frac{\partial}{\partial \boldsymbol{\xi}} \mathbf{f}(\mathbf{V}) = \mathbf{0}. \tag{21}$$

We first introduce a class of numerical schemes for computing the basic solution $\mathbf{V}$ to (21). Given a mesh size $\Delta\xi_j$ and a time step Δt, we define an approximation $\mathbf{V}_j^n$ of $\mathbf{V}(\xi_j, t^n)$ at the point (ξ_j, t^n). The one-step (in time) explicit scheme takes the following form:

$$\mathbf{V}_j^{n+1} = \mathbf{V}_j^n - \frac{\Delta t}{\Delta \xi_j} \left(\mathbf{f}(\mathbf{V})_{j+\frac{1}{2}}^n - \mathbf{f}(\mathbf{V})_{j-\frac{1}{2}}^n \right), \tag{22}$$

where $\mathbf{f}(\mathbf{V})_{j+\frac{1}{2}}^n$ is the numerical flux that we propose to discuss now. Letting

$$\psi = \begin{pmatrix} p \\ -u \end{pmatrix}, \quad \mathbf{B} = \begin{pmatrix} 0 & 1 \\ 1 & 0 \end{pmatrix}, \tag{23}$$

it is a simple matter to check that the lagrangian flux (17) can be rewritten as

$$\mathbf{f}(\mathbf{V}) = \begin{pmatrix} \mathbf{B}\psi \\ -\frac{1}{2}\psi^{\mathrm{t}}\mathbf{B}\psi \end{pmatrix}. \tag{24}$$

This formula has an important consequence in terms of numerical schemes: instead of studying the Jacobian matrix $\mathrm{d}\mathbf{f}/\mathrm{d}\mathbf{V}$ which is a 3×3 non constant matrix, [1] it is sufficient to study the 2×2 constant matrix $\mathbf{B}$. This has already been noticed by Després [9] who proposed a class of numerical schemes for solving (21). The idea is the following: at each interface $j + \frac{1}{2}$ the matrix $\mathbf{B}$ is split into a positive part $\mathbf{B}_{j+\frac{1}{2}}^+$ and a negative part $\mathbf{B}_{j+\frac{1}{2}}^-$:

$$\mathbf{B} = \mathbf{B}_{j+\frac{1}{2}}^+ + \mathbf{B}_{j+\frac{1}{2}}^-, \quad \text{with} \quad \mathbf{B}_{j+\frac{1}{2}}^+ \geqslant 0, \quad \text{and} \quad \mathbf{B}_{j+\frac{1}{2}}^- \leqslant 0. \tag{25}$$

[1] This is typically the case when using the Roe method.

The numerical flux is therefore given by

$$\mathbf{f}(\mathbf{V})^n_{j+\frac{1}{2}} = \begin{pmatrix} \mathbf{B}^+_{j+\frac{1}{2}}\psi^n_{j+1} + \mathbf{B}^-_{j+\frac{1}{2}}\psi^n_j \\ -\frac{1}{2}\left(\psi^n_{j+1}\right)^{\mathrm{t}}\mathbf{B}^+_{j+\frac{1}{2}}\psi^n_{j+1} - \frac{1}{2}\left(\psi^n_j\right)^{\mathrm{t}}\mathbf{B}^-_{j+\frac{1}{2}}\psi^n_j \end{pmatrix}, \tag{26}$$

where the choice of ψ^n_{j+1} or ψ^n_j for the "up-winding" is made accordingly to the sign of $\mathbf{B}^{\pm}$. For this class of schemes, it has been proved that when the matrices $\mathbf{B}^{\pm}$ are symmetric, the scheme (22), (23), (25) and (26) is entropic under CFL condition [9, Theorem 2].

It is to be noticed that choosing a splitting for $\mathbf{B}$ is equivalent to building an approximate Riemann solver. We now give an example that will be used in the sequel: the approximate Riemann solver of Després [9]. This approximate Riemann solver is a variant of the Godunov acoustic solver [15] in which the speed of sound has been frozen: $(\rho c)^n_j = (\rho c)^n_{j+1} = (\rho c)^*_{j+\frac{1}{2}}$. Therefore, at each interface $\xi_{j+\frac{1}{2}}$ the pressure $p^*_{j+\frac{1}{2}}$ and the velocity $u^*_{j+\frac{1}{2}}$ are given by

$$\begin{cases} u^*_{j+\frac{1}{2}} = \frac{u^n_j + u^n_{j+1}}{2} + \frac{1}{2(\rho c)^*_{j+\frac{1}{2}}}\left(p^n_j - p^n_{j+1}\right), \\ p^*_{j+\frac{1}{2}} = \frac{p^n_j + p^n_{j+1}}{2} + \frac{(\rho c)^*_{j+\frac{1}{2}}}{2}\left(u^n_j - u^n_{j+1}\right). \end{cases} \tag{27}$$

In terms of matrix splitting this is equivalent to

$$\mathbf{B}^{\pm}_{j+\frac{1}{2}} = \begin{pmatrix} \pm\frac{1}{2(\rho c)^*_{j+\frac{1}{2}}} & \frac{1}{2} \\ \frac{1}{2} & \pm\frac{(\rho c)^*_{j+\frac{1}{2}}}{2} \end{pmatrix}. \tag{28}$$

As it has been reported in previous studies [8,9], the closer $(\rho c)^*_{j+\frac{1}{2}}$ is to the local Lagrangian speed of sound, the better the time step is. A good choice is given by

$$(\rho c)^*_{j+\frac{1}{2}} = \sqrt{\frac{\max\left(\rho^n_j (c^n_j)^2, \rho^n_{j+1}(c^n_{j+1})^2\right)}{\max\left(1/\rho^n_j, 1/\rho^n_{j+1}\right)}}. \tag{29}$$

With this definition, it is a simple matter to prove that $(\rho c)^*_{j+\frac{1}{2}}$ satisfies the following inequality:

$$\min\left((\rho c)^2_j, (\rho c)^2_{j+1}\right) \leqslant ((\rho c)^*_{j+\frac{1}{2}})^2 \leqslant \max\left((\rho c)^2_j, (\rho c)^2_{j+1}\right).$$

The resulting scheme is then entropic under the CFL condition:

$$\max_j \overline{\rho c}_j \frac{\Delta t}{\Delta \xi_j} \leqslant 1, \tag{30a}$$

with

$$\overline{\rho c}_j = \max\left(\frac{(\rho c)^*_{j-\frac{1}{2}} + (\rho c)^*_{j+\frac{1}{2}}}{2}, \left(\frac{1}{(\rho c)^*_{j-\frac{1}{2}}} + \frac{1}{(\rho c)^*_{j+\frac{1}{2}}}\right)\frac{(\rho c)^2_j}{2}\right). \tag{30b}$$

3.2. Numerical schemes for the linearized flow

Using the formalism described in the preceding section, we propose to discretize (18a) satisfied by $\hat{\mathbf{V}}$, namely

$$\frac{\partial \hat{\mathbf{V}}}{\partial t} + \frac{\partial}{\partial \xi}\left\{ \frac{\mathrm{d}\mathbf{f}}{\mathrm{d}\mathbf{V}}(\mathbf{V})\hat{\mathbf{V}} \right\} = \mathbf{S}\left(\mathbf{V}, \hat{\Omega}, \hat{\Theta}\right), \tag{31a}$$

where

$$\mathbf{S}\left(\mathbf{V}, \hat{\Omega}, \hat{\Theta}\right) = -\frac{\partial}{\partial \xi}\mathbf{f}(\mathbf{V})\hat{\Theta} + \tau\hat{\Omega}\begin{pmatrix} 1 \\ 0 \\ -p \end{pmatrix}, \tag{31b}$$

by a Godunov-type scheme of the form

$$\hat{\mathbf{V}}_j^{n+1} = \hat{\mathbf{V}}_j^n - \frac{\Delta t}{\Delta \xi_j}\left(\mathbf{g}\left(\mathbf{V}, \hat{\mathbf{V}}\right)^n_{j+\frac{1}{2}} - \mathbf{g}\left(\mathbf{V}, \hat{\mathbf{V}}\right)^n_{j-\frac{1}{2}} \right) + \Delta t \mathbf{S}\left(\mathbf{V}, \hat{\Omega}, \hat{\Theta}\right)^n_j, \tag{32}$$

where $\mathbf{g}(\mathbf{V}, \hat{\mathbf{V}})^n_{j+\frac{1}{2}}$, which is consistent with $\mathrm{d}\mathbf{f}(\mathbf{V})/\mathrm{d}\mathbf{V}\hat{\mathbf{V}}$, is the linearized numerical flux.

From what has been done in the preceding section, the discretization of the source term is simply given by

$$\mathbf{S}\left(\mathbf{V}, \hat{\Omega}, \hat{\Theta}\right)^n_j = -\frac{1}{\Delta \xi_j}\left(\mathbf{f}(\mathbf{V})^n_{j+\frac{1}{2}} - \mathbf{f}(\mathbf{V})^n_{j-\frac{1}{2}} \right)\hat{\Theta}^n_j + \tau^n_j \hat{\Omega}^n_j \begin{pmatrix} 1 \\ 0 \\ -p^n_j \end{pmatrix}, \tag{33}$$

where $\mathbf{f}(\mathbf{V})^n_{j+\frac{1}{2}}$ is defined by (26).

We are now interested in the discretization of the linearized flux $\mathbf{g}(\mathbf{V}, \hat{\mathbf{V}})$. First, we note that the Fourier transform of the linearized perturbation of ψ is given by $\hat{\psi} = \mathrm{d}\psi(\mathbf{V})/\mathrm{d}\mathbf{V}\hat{\mathbf{V}}$. Therefore, using (24) and since $\mathbf{B}$ is a constant symmetric matrix, we have

$$\mathbf{g}\left(\mathbf{V}, \hat{\mathbf{V}}\right) = \frac{\mathrm{d}\mathbf{f}}{\mathrm{d}\psi}\frac{\mathrm{d}\psi}{\mathrm{d}\mathbf{V}}(\mathbf{V})\hat{\mathbf{V}} = \frac{\mathrm{d}\mathbf{f}}{\mathrm{d}\psi}(\psi)\hat{\psi} = \begin{pmatrix} \mathbf{B}\hat{\psi} \\ -\psi^{\mathrm{t}}\mathbf{B}\hat{\psi} \end{pmatrix}.$$

In order to derive the numerical flux $\mathbf{g}(\mathbf{V}, \hat{\mathbf{V}})^n_{j+\frac{1}{2}}$ we simply use the matrix splitting (25) and the same "upwinding" as for the basic flow:

$$\mathbf{g}\left(\mathbf{V}, \hat{\mathbf{V}}\right)^n_{j+\frac{1}{2}} = \begin{pmatrix} \mathbf{B}^+_{j+\frac{1}{2}}\hat{\psi}^n_{j+1} + \mathbf{B}^-_{j+\frac{1}{2}}\hat{\psi}^n_j \\ -\left(\psi^n_{j+1}\right)^{\mathrm{t}}\mathbf{B}^+_{j+\frac{1}{2}}\hat{\psi}^n_{j+1} - \left(\psi^n_j\right)^{\mathrm{t}}\mathbf{B}^-_{j+\frac{1}{2}}\hat{\psi}^n_j \end{pmatrix} = \begin{pmatrix} -\hat{u}^*_{j+\frac{1}{2}} \\ \hat{p}^*_{j+\frac{1}{2}} \\ p^*_{j+\frac{1}{2}}\hat{u}^*_{j+\frac{1}{2}} + u^*_{j+\frac{1}{2}}\hat{p}^*_{j+\frac{1}{2}} \end{pmatrix}, \tag{34}$$

where $\mathbf{B}^{\pm}$ are exactly the matrices used to compute the basic solution.

Finally, the differential equations (18b–d) are integrated using the following explicit finite difference scheme:

$$\hat{\Omega}^{n+1}_j = \hat{\Omega}^n_j + \Delta t k_\perp^2 \left(\tau^n_j \hat{p}^n_j - \frac{p^*_{j+\frac{1}{2}}\hat{x}^n_{j+\frac{1}{2}} - p^*_{j-\frac{1}{2}}\hat{x}^n_{j-\frac{1}{2}}}{\Delta \xi_j} + \frac{\hat{x}^n_{j+\frac{1}{2}} - \hat{x}^n_{j-\frac{1}{2}}}{\Delta \xi_j} p^n_j \right), \tag{35a}$$

$$\hat{x}^{n+1}_{j+\frac{1}{2}} = \hat{x}^n_{j+\frac{1}{2}} + \Delta t \hat{u}^*_{j+\frac{1}{2}}, \tag{35b}$$

$$\hat{\Theta}^{n+1}_j = \hat{\Theta}^n_j + \Delta t \hat{\Omega}^n_j. \tag{35c}$$

Remark 1. It is worth noticing that all Lagrangian systems of conservation laws with zero entropy flux corresponding to fluid models can be rewritten in the form

$$\frac{\partial \mathbf{V}}{\partial t}+\frac{\partial}{\partial \xi}\begin{pmatrix}\mathbf{B}\psi\\ -\frac{1}{2}\psi^{\mathrm{t}}\mathbf{B}\psi\end{pmatrix}=\mathbf{0},$$

where $\mathbf{B}$ is a constant symmetric matrix and ψ the reduced entropic variable (see [9, Theorem 1]). Therefore the ideas exposed here in the context of gas dynamics are immediately applicable to more complex systems, such as a two-temperature fluid model, ideal magnetohydrodynamics, certain models of radiative hydrodynamics or of elasto-plasticity, etc. This same property is also responsible for the remarkable simplicity of the numerical flux linearization procedure, a feature not granted by the Roe scheme linearization of [28].

Remark 2. As previously mentioned at the beginning of Section 3, a Godunov-type method based on a Roe solver has already been developed in [28] for solving (16) and (18). It has been proved in [20] that, in the context of gas dynamics, the flux (26) can be reinterpreted as a Roe flux, nevertheless the linearized versions of these schemes are different [20].

3.3. Extension to second-order accurate schemes

Two standard approaches for increasing the order of accuracy of the above Godunov-type methods have been tested: one relies on flux limiting and a Lax–Wendroff-type scheme [21], the other uses MUSCL variable extrapolations (e.g. see [33]) in conjunction with a third order Runge–Kutta method [32].

3.3.1. The Lax–Wendroff scheme using flux limiters

The momentum and the energy equations of the basic flow can be manipulated to give, in a non conservative form:

$$\begin{cases}\frac{\partial u}{\partial t}+\frac{\partial p}{\partial \xi}=0,\\ \frac{\partial p}{\partial t}+(\rho c)^2\frac{\partial u}{\partial \xi}=0.\end{cases}$$

A Lax–Wendroff-type scheme is applied over a half-time step $\Delta t/2$ (we refer to [1] for further details) thus giving a second-order approximation of the velocity and the pressure at each interface $\xi_{j+\frac{1}{2}}$, respectively denoted $u^{*,\mathrm{LW}}_{j+\frac{1}{2}}$ and $p^{*,\mathrm{LW}}_{j+\frac{1}{2}}$. This solver, say $u^{*,\mathrm{HI}}$ and $p^{*,\mathrm{HI}}$, is connected to the first order one, $u^{*,\mathrm{LO}}$ and $p^{*,\mathrm{LO}}$, *via* a Van Leer flux limiter Φ (cf. [33]):

$$\begin{cases}u^{*,\mathrm{HI}}=\Phi u^{*,\mathrm{LO}}+(1-\Phi)u^{*,\mathrm{LW}},\\ p^{*,\mathrm{HI}}=\Phi p^{*,\mathrm{LO}}+(1-\Phi)p^{*,\mathrm{LW}},\end{cases}\tag{36}$$

which reads, in an extended form

$$\begin{cases}u^*_{j+\frac{1}{2}}=\frac{u^n_j+u^n_{j+1}}{2}+\Phi\frac{1}{2(\rho c)^*_{j+\frac{1}{2}}}\left(p^n_j-p^n_{j+1}\right)+(1-\Phi)\frac{\Delta t}{2}\frac{p^n_j-p^n_{j+1}}{\frac{1}{2}(\Delta\xi_j+\Delta\xi_{j+1})},\\ p^*_{j+\frac{1}{2}}=\frac{p^n_j+p^n_{j+1}}{2}+\Phi\frac{(\rho c)^*_{j+\frac{1}{2}}}{2}\left(u^n_j-u^n_{j+1}\right)+(1-\Phi)\frac{\Delta t}{2}\left((\rho c)^*_{j+\frac{1}{2}}\right)^2\frac{u^n_j-u^n_{j+1}}{\frac{1}{2}(\Delta\xi_j+\Delta\xi_{j+1})}.\end{cases}$$

Since the linearized flow satisfies a linear system of conservation laws, we infer that no flux limiting techniques should be necessary for computing the linear perturbation. The situation is in fact much more complex, because the perturbed flow is solution to a linear system of conservation laws with discontinuous coefficients. In practice (see Section 4.3) the same limiter as for the basic flow is applied. Therefore, the second-order scheme for computing the linearized solution corresponds to (32) where $\mathbf{S}(\mathbf{V},\hat{\Omega},\hat{\Theta})^n_j$ is discretized by (33) in which $\mathbf{f}(\mathbf{V})^n_{j+\frac{1}{2}}$ is the basic second-order flux defined by (36), while the second-order linearized flux $\mathbf{g}(\mathbf{V},\hat{\mathbf{V}})^n_{j+\frac{1}{2}}$ is given by (36) with $\hat{u}^n_i$ and $\hat{p}^n_i$ in place of, respectively, u^n_i and p^n_i (for $i=j,j+1$).

3.3.2. MUSCL-type schemes

MUSCL-type schemes are here constructed by introducing piecewise linear distributions in each computational cell, not only – as is usual (e.g. see [33]) – for some basic flow dependent variables $\mathbf{Q}$,

$$\mathbf{Q}^n(\xi) = \mathbf{Q}_j^n + \Delta\mathbf{Q}_j^n(\xi - \xi_j), \quad \xi_{j-\frac{1}{2}} < \xi < \xi_{j+\frac{1}{2}}, \tag{37}$$

but also for dependent variable linear perturbation Fourier components, say $\hat{\mathcal{Q}}$,

$$\hat{\mathcal{Q}}^n(\xi) = \hat{\mathcal{Q}}_j^n + \Delta\hat{\mathcal{Q}}_j^n(\xi - \xi_j), \quad \xi_{j-\frac{1}{2}} < \xi < \xi_{j+\frac{1}{2}}. \tag{38}$$

The cell-edge extrapolated values of the dependent variable pair $(\mathbf{Q}, \hat{\mathcal{Q}})$, as defined by these linear distributions, are then used for evaluating the numerical fluxes (26) and (34) in (22) and (32). Note that $\hat{\mathcal{Q}}$ may not necessarily correspond to $\hat{\mathbf{Q}}$, the linear perturbation Fourier components of $\mathbf{Q}$. In practice, the slopes $\Delta\mathbf{Q}_j^n$ in (37) are determined by applying the classical MINMOD slope-limiting function. As in the case of the Lax–Wendroff-type scheme, the same slope-limiting process is here used for computing the slope $\Delta\hat{\mathcal{Q}}_j^n$ in (38). Two distinct pairs of dependent variables $(\mathbf{Q}, \hat{\mathcal{Q}})$ have been routinely tested. The first pair corresponds to what is known as "slope limiting in local characteristic variables" for $\mathbf{Q}$ and its linearized version for $\hat{\mathcal{Q}}$. This variable extrapolation presents the advantage of yielding results which are less oscillatory than those obtained with other choices for $\mathbf{Q}$, a feature especially desirable when computing solutions of (32). The other pair is given by the primitive variables $\mathbf{Q} = (\tau, u, \mathscr{E})^{\mathrm{t}}$ and their linear perturbations $\hat{\mathcal{Q}} = (\hat{\tau}, \hat{u}, \hat{\mathscr{E}})^{\mathrm{t}}$, this latter choice being exclusively used when the previous extrapolation method fails to guarantee the positivity of extrapolated specific internal energy values.

4. Numerical results

As an illustration of the above numerical method capabilities to produce quantitative results for instabilities of shocked multi-material flows, we have chosen to consider the Richtmyer–Meshkov instability. Richtmyer–Meshkov instabilities occur when a planar shock wave collides, at normal incidence, with an imperfectly flat interface separating two different fluids: interface perturbations grow following the shock-interface interaction [29,25]. For sufficiently small perturbation amplitudes this growth is asymptotically linear in time. In the absence of perturbations, the flow is simply a one-dimensional shock-contact discontinuity interaction. For a perturbed interface, geometrical defect amplitudes grow as the result of the shear flow initiated by the complex interaction of the incident planar shock wave with the corrugated interface. Hence, numerical computations of Richtmyer–Meshkov instabilities are particularly sensitive to shock-contact approximation errors such as "wall-heating" effects, numerical smearing of contact discontinuities, and the ability to accurately describe shear motions.

In the following, we detail linear perturbation computation results of Richtmyer–Meshkov instabilities involving two perfect gases of different adiabatic exponents, in the two cases of a reflected shock wave (Section 4.1) and of a reflected rarefaction wave (Section 4.2). We then summarize (Section 4.3) the results of a quantitative comparison – in terms of interface perturbation asymptotic growth rates – of our linear perturbation calculations with the Richtmyer–Meshkov instability linear theory [35]. Although this comparison is exclusively based on interface perturbation growth rates, one should keep in mind that, in complex flow stability studies, one is in fact interested in the detailed spatial and temporal behaviors of perturbations. Such detailed descriptions which are readily available from linear perturbation calculations, are way more arduous to extract from 2D/3D simulations.

Basic flow initial conditions. Herein the basic flow initial conditions are defined as

$$\mathbf{V}_0^0(\xi) = \begin{cases} \mathbf{V}_\mathrm{L}^\mathrm{s}, & \text{if } \xi_{\min} < \xi < \xi_\mathrm{s}, \\ \mathbf{V}_\mathrm{L}^\mathrm{u}, & \text{if } \xi_\mathrm{s} < \xi < \xi_\Sigma, \\ \mathbf{V}_\mathrm{R}, & \text{if } \xi_\Sigma < \xi < \xi_{\max}, \end{cases}$$

where ξ_Σ denotes the location of the interface between the two fluids, ξ_s that of the incident shock-wave front which propagates from the L-fluid to the R-fluid, while $\mathbf{V}_\mathrm{L}^\mathrm{s}$ and $\mathbf{V}_\mathrm{L}^\mathrm{u}$ are respectively the shocked and unshocked states of the L-fluid.

Both fluids being governed by perfect-gas equations of state – of adiabatic exponents γ_L and γ_R for, respectively, the L- and R-fluid – the states $\mathbf{V}_\mathrm{L}^\mathrm{u}$ and $\mathbf{V}_\mathrm{R}$ are taken to be

$$\mathbf{V}_\mathrm{L}^\mathrm{u} = \begin{cases} \rho_\mathrm{L}^\mathrm{u} = 1, \\ u_\mathrm{L}^\mathrm{u} = 0, \\ p_\mathrm{L}^\mathrm{u} = 1, \end{cases} \quad \mathbf{V}_\mathrm{R} = \begin{cases} \rho_\mathrm{R} = \alpha, \\ u_\mathrm{R} = 0, \\ p_\mathrm{R} = 1, \end{cases}$$

where α is a parameter of the problem. In addition, we introduce the strength of the incident shock, $s = 1 - p_\mathrm{L}^\mathrm{u}/p_\mathrm{L}^\mathrm{s}$, whose value defines the shocked state $\mathbf{V}_\mathrm{L}^\mathrm{s}$ *via* the Rankine–Hugoniot jump relations.

Linear perturbation initial conditions. Given the above definition of the basic flow initial conditions, linear perturbation initial conditions are given as compact support solutions of Eq. (C.3) and of the boundary value problems (C.5) and (C.6) introduced in Appendix C. For convenience, the initial perturbation amplitude of the material discontinuity surface is chosen to be of unit length: $\widehat{\phi_S} = 1$ in (C.5) and (C.6). Letting $[\xi_a, \xi_b]$, with $\xi_{\min} < \xi_a < \xi_\Sigma < \xi_b < \xi_{\max}$, denote the compact support of these initial conditions, we take, for a given spatial discretization $(\xi_{j+\frac{1}{2}})$ of the interval $[\xi_{\min}, \xi_{\max}]$, the values of ξ_a and ξ_b to be such that

$$\xi_{j_*+\frac{1}{2}} - \xi_a < \Delta\xi_{j_*}, \quad \text{and} \quad \xi_b - \xi_{j_*+\frac{1}{2}} < \Delta\xi_{j_*+1},$$

where $\xi_{j_*+\frac{1}{2}} = \xi_\Sigma$ is the cell edge corresponding to the material contact discontinuity. Consequently, the discrete approximation of the solutions $(\hat{x}_0, \hat{\Theta}_0)$ to the boundary value problems (C.5) and (C.6) is given by

$$\hat{x}_{0,j+\frac{1}{2}} = \begin{cases} 1 & \text{for } j = j_*, \\ 0 & \text{otherwise}, \end{cases} \quad \text{with} \quad \hat{\Theta}_{0,j} = \frac{\hat{x}_{0,j-\frac{1}{2}} - \hat{x}_{0,j+\frac{1}{2}}}{\Delta x_j}. \tag{39}$$

We note that although the solutions $(\hat{x}_0, \hat{\Theta}_0)$ of (C.5) and (C.6) have not been explicitly given, their discrete approximation (39) is uniquely defined. These definitions are completed by the equalities $\hat{\mathbf{V}}_{0,j} = \mathbf{0}$ and $\hat{\Omega}_{0,j} = 0$ stemming from Eq. (C.3) and from the fact that the fluids are initially at rest. From a practical standpoint, such discrete initial conditions are more convenient to handle than a discrete form of the Dirac measure initial conditions of [13, Eq. (46)].

Numerical growth rates. In Lagrangian coordinates, the contact discontinuity is stationary. Therefore one may easily determine the numerical growth rate of the Richtmyer–Meshkov instability, say ω, by means of the relation

$$\omega(t_n) = \frac{\mathrm{d}\hat{x}}{\mathrm{d}t}\left(\xi_{j_*+\frac{1}{2}}, t_n\right) = \hat{u}\left(\xi_{j_*+\frac{1}{2}}, t_n\right) = \hat{u}^*_{j_*+\frac{1}{2}}.$$

However in order to minimize the uncertainties due to oscillations in the velocity profiles (see Figs. 3 and 7) when determining these velocities, we have computed numerically the slopes of $\hat{x}_{j_*+\frac{1}{2}}(t)$ by means of a least-square fit. Note that, in the sequel, we will in fact refer to what is called in the literature the *normalized growth rate*, defined by (see [35])

$$\omega_{\mathrm{NGR}} = \frac{\omega}{k_\perp \sigma},$$

where $k_\perp$ is the perturbation transverse wavenumber and σ the Eulerian speed of the incident shock wave.

4.1. Case of a reflected shock wave

In regards to [13], the interest of our numerical method is its ability to take into account two fluids governed by different equations of state. Considering the adiabatic exponent pair $(\gamma_L, \gamma_R) = (1.5, 3)$, and the parameter values $\alpha = 4$, $s = 0.5$, it can be proved that the reflected and transmitted waves, resulting from the shock-interface interaction, are both shock waves. Fig. 1 gives the density profiles of the basic flow at $t = 0$ and $t = 3$ in Eulerian coordinates, Fig. 2 the profile of linear perturbations at $t = 3$ and Fig. 3 the time evolutions of the perturbed longitudinal speed and perturbed amplitude at the interface.

It has been shown in [13] (see Remark 1 and Eq. (B.9)) that the linear perturbation writes

$$\hat{\mathbf{V}}(\xi, t) = \left\{\hat{\mathbf{V}}(\xi, t)\right\} + \sum_{j=1}^{3} \hat{\psi}_j [\mathbf{V}^0] \delta_{\Sigma_j},$$

i.e. as the sum of a function $\{\hat{\mathbf{V}}(\xi, t)\}$ and of Dirac masses carried by the discontinuity lines Σ_j of the basic flow, which is exactly what is shown in Fig. 2. Note that since $[u^0] = [p^0] = 0$ across the interface Σ_2, Dirac masses on $\hat{u}$ and $\hat{p}$ are not present at this interface. Nevertheless they are visible on the reflected (Σ_1) and transmitted (Σ_3) shock fronts. These Dirac masses interact with the acoustic waves that propagate between these two shocks. We clearly see the perturbation growth at the interface (especially on $\hat{x}$).

Fig. 3 shows the time evolution of the normalized perturbed longitudinal speed at the interface, $\hat{u}/(k_\perp \sigma)$. We clearly see regular oscillations (of acoustic origin) about a mean value which corresponds to those predicted by the impulsive model of Vandenboomgaerde et al. [34] or by the linear theory developed by Yang et al. [35]. The profile of the time evolution of the perturbation amplitude is even more significant. Before the shock front hits the interface (which happens at $t \simeq 0.8$), the amplitude of the perturbation is $a_0^- = 1$. Right after the interaction, this amplitude theoretical value is $a_0^+ = (1 - \Delta u/\sigma) a_0^-$ (see [34] for instance), while the ongoing amplitude evolution becomes clearly linear. The normalized growth rate obtained in this case is $\omega_{NGR} = 0.1004$ (which is to be compared to $\omega_{NGR} = 0.098$ for the impulsive model [34] and $\omega_{NGR} = 0.1$ for the linear theory [35]).

In addition, we have performed a convergence study, giving the growth rate of the perturbation with respect to the number of cells per unit of transverse wavelength, for first- and second-order schemes (Fig. 4). This study shows that in order to get less than 5% of relative error, we must use at least 400 (respectively 100) cells per unit of transverse wavelength with the first- (respectively second-) order scheme.

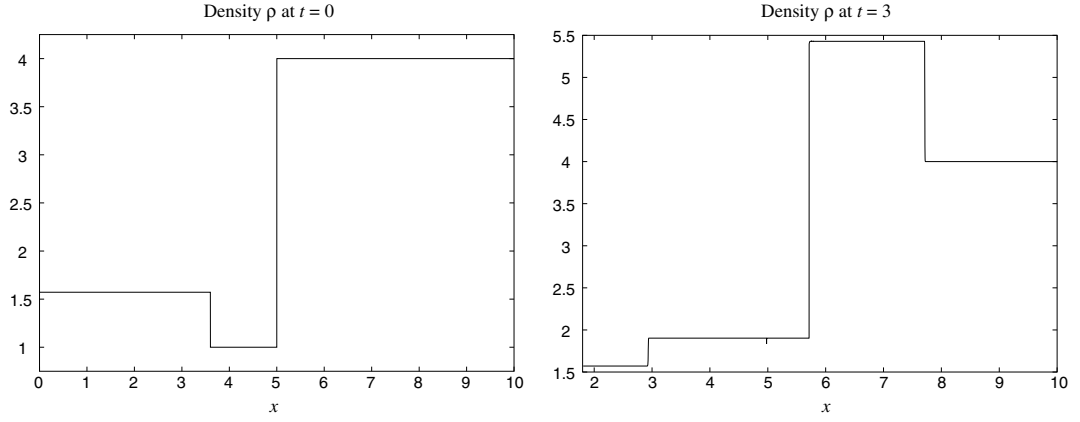

Fig. 1. Density profiles of the basic flow at $t = 0$ (left) and $t = 3$ (right). The reflected wave is a shock wave. Parameters are $\gamma_L = 1.5$, $\gamma_R = 3$, $\alpha = 4$ and $s = 0.5$.

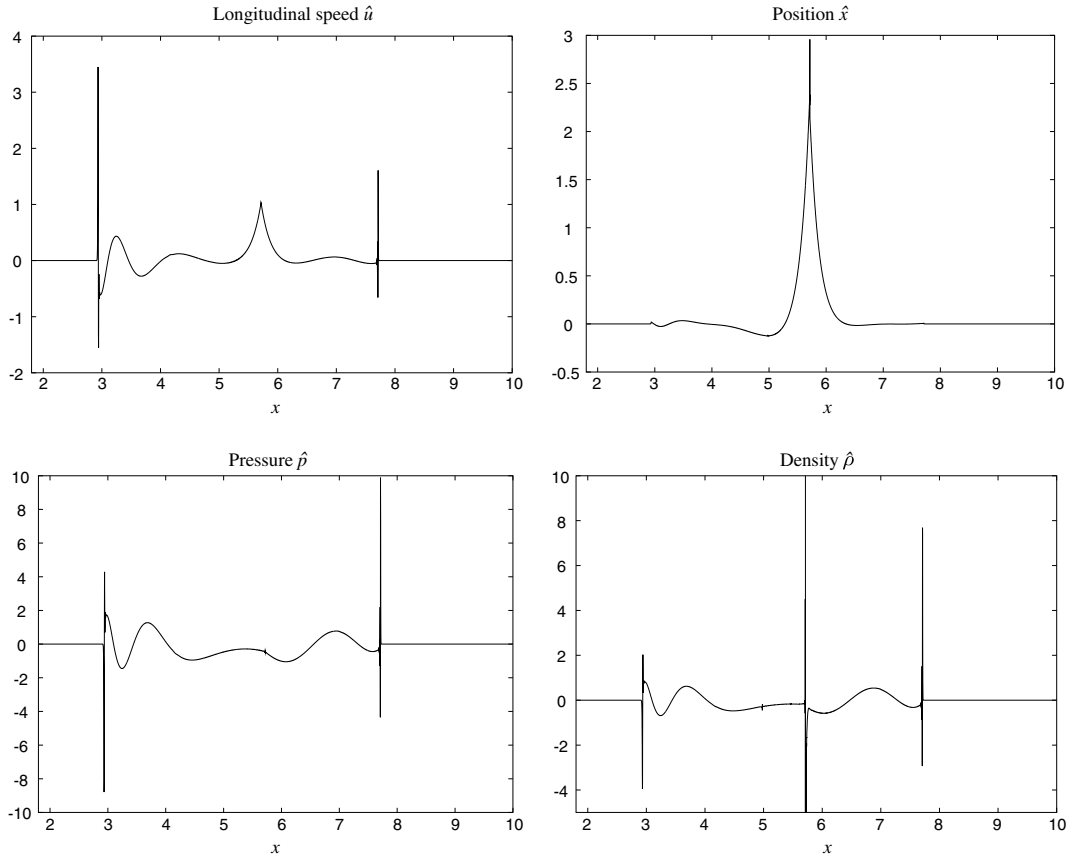

Fig. 2. Perturbation profiles at $t = 3$. The interface is located at $x \simeq 5.7$. Parameters are given by $\gamma_L = 1.5$, $\gamma_R = 3$, $\alpha = 4$ and $s = 0.5$.

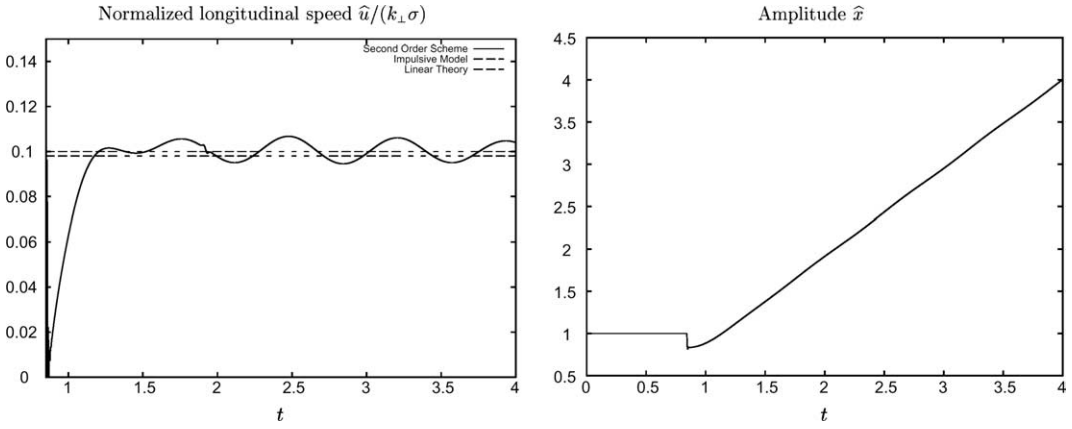

Fig. 3. Time evolutions of the normalized perturbed longitudinal speed (left) and amplitude (right) at the interface. Horizontal lines (left) are the normalized growth rates obtained by Vandenboomgaerde et al. [34] and by Yang et al. [35]. Parameters are given by $\gamma_L = 1.5$, $\gamma_R = 3$, $\alpha = 4$ and $s = 0.5$.

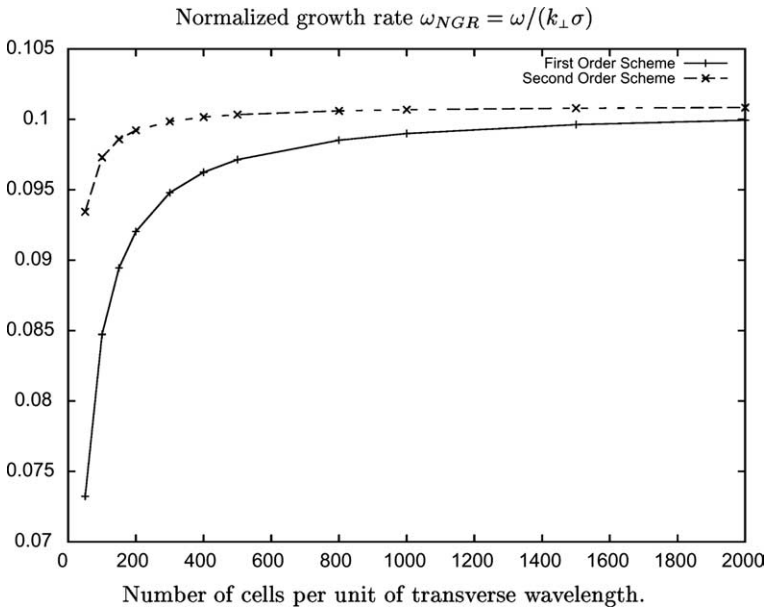

Fig. 4. Convergence study. Normalized growth rates as given by the first- (—) and second- (– –) order schemes vs. the number of cells per unit of transverse wavelength.

4.2. Case of a reflected rarefaction wave

For the adiabatic exponent pair $(\gamma_L, \gamma_R) = (3, 1.5)$, and the parameter values $\alpha = 0.25$, $s = 0.5$, the reflected wave is a rarefaction wave. Fig. 5 shows the density profiles of the basic flow at $t = 0$ and $t = 2$. We clearly see these two waves together with the contact discontinuity.

Fig. 6 gives the profiles of perturbations at $t = 2$. Comments are similar to those made for Fig. 3: perturbations are sums of functions and Dirac masses carried by the discontinuity lines of the basic flow. Since the reflected wave is a rarefaction wave – which is regular – no Dirac masses appear about this wave.

Fig. 7 gives the time evolution of the perturbed (normalized) longitudinal speed and of the perturbation amplitude at the interface. The growth rate obtained with our method is in agreement with those we have found in the literature: we find $\omega_{NGR} = -0.14003$, which is to be compared with the value $\omega_{NGR} = -0.14$ of the impulsive model [34] and of the linear theory [35]. The $\hat{x}$-profile is similar to that of Fig. 3. Furthermore we have access to the compression factor linking the pre-shocked and post-shocked amplitudes a_0^- and a_0^+.

4.3. Comparisons of normalized growth rates

We have performed many numerical tests in order to compare the growth rates obtained with our approach together with those predicted by the impulsive model of Vandenboomgaerde et al. [34] and those computed from the linear theory of Yang et al. [35]. The results of these comparisons are summarized in Table 1 for the cases of reflected shock waves, and in Table 2 for the cases of reflected rarefaction waves.

Varying parameters are the adiabatic exponents γ_L and γ_R, the incident shock strength s and the pre-shocked density ratio $\alpha = \rho_R/\rho_L^u$. For each entry the first two values are those given respectively by the

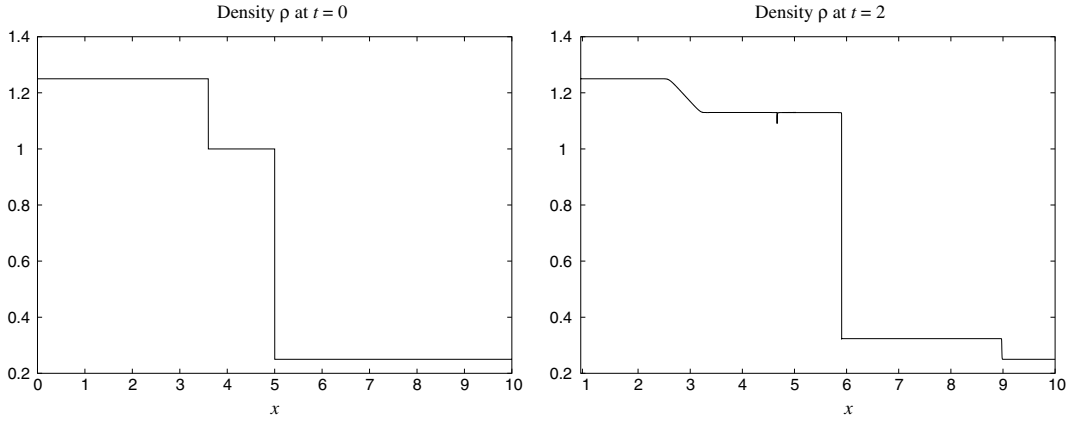

Fig. 5. Density profiles of the basic flow at $t = 0$ (left) and $t = 2$ (right). The reflected wave is a rarefaction wave. Parameters are given by $\gamma_L = 3$, $\gamma_R = 1.5$, $\alpha = 0.25$ and $s = 0.5$.

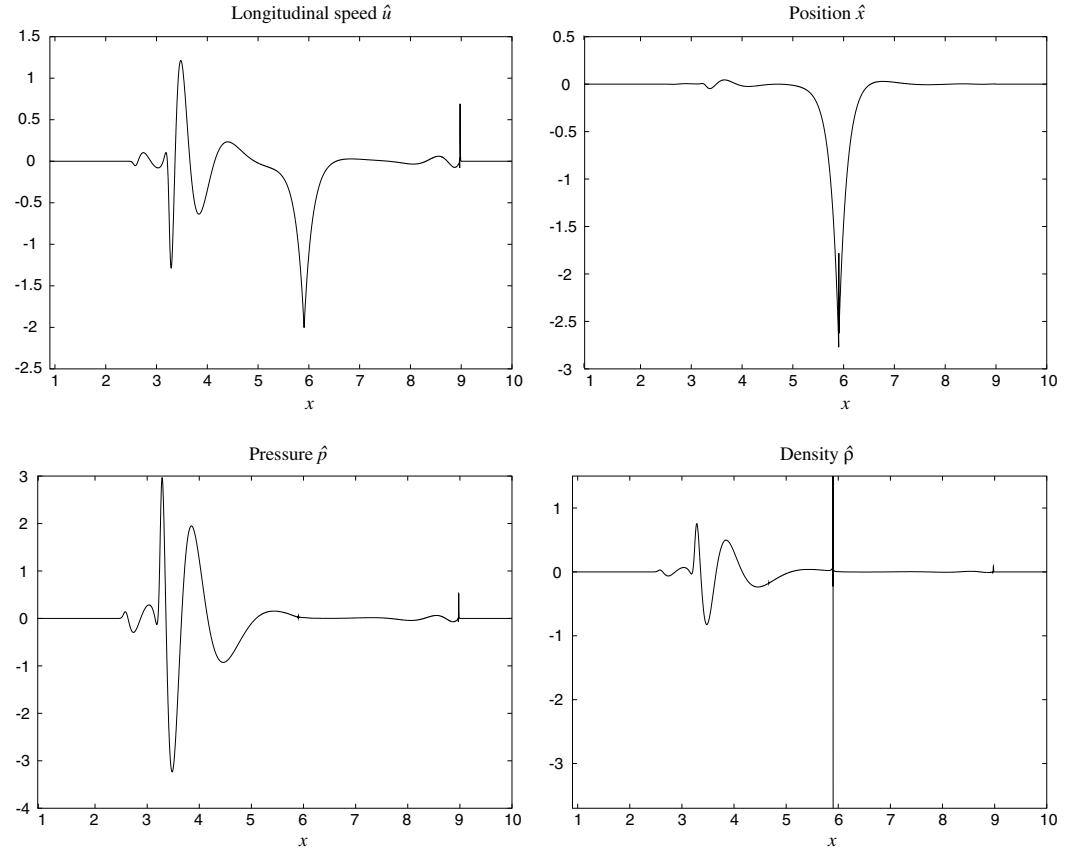

Fig. 6. Perturbation profiles at $t = 2$. The interface is located at $x \simeq 5.8$. Parameters are given by $\gamma_L = 3$, $\gamma_R = 1.5$, $\alpha = 0.25$ and $s = 0.5$.

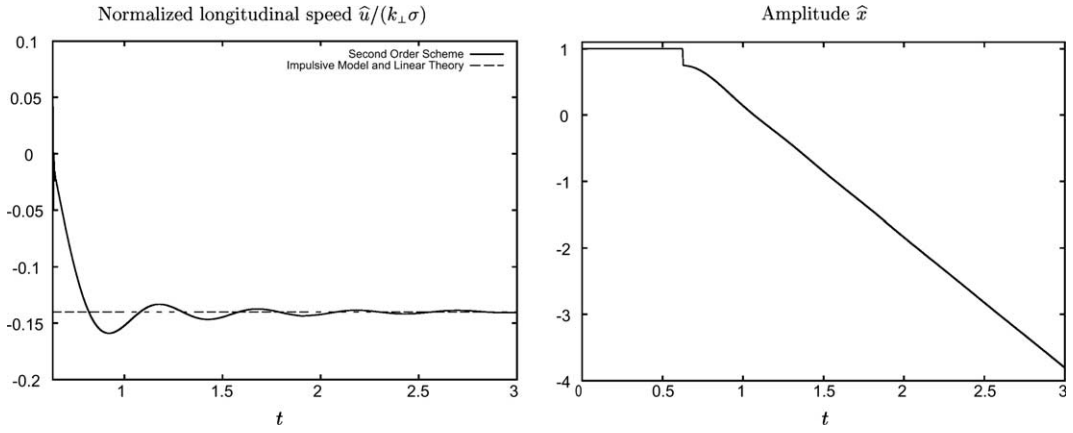

Fig. 7. Time evolutions of the normalized perturbed longitudinal speed (left) and amplitude (right). The horizontal line (left) is the normalized growth rate obtained by Vandenboomgaerde et al. [34] and by Yang et al. [35]. Parameters are given by $\gamma_L = 3$, $\gamma_R = 1.5$, $\alpha = 0.25$ and $s = 0.5$.

impulsive model [34] and the linear theory of Yang et al. [35], while the third one is that obtained with our second-order schemes using 500 cells per unit of transverse wavelength.

Through these two tables we observe a good agreement, in general, between our results and those obtained by the linear theory of Yang et al. [35] and, to a lesser extent, with those of the impulsive model [34]. Results are more especially closer as the shock strength decreases and as the adiabatic exponents are large – a fact noticed in [34], the authors stating therein that the impulsive model gives a fairly good approximation of the growth rate within its domain of validity: $s \leqslant 0.4$ and $\gamma_{max}/\gamma_{min} \leqslant 1.5$. This fact had already been mentioned in [35].

Discrepancies between our computed results and those of the linear theory [35] are most noticeable for some of the moderate ($s = 0.5$) and large ($s = 1$) shock strength configurations – see, for example, the entries of Table 1 or Table 2 when $s = 1$, in the cases of:

- $(\gamma_L, \gamma_R) = (1.1, 1.1)$, for $\rho_R/\rho_L^u = 16$ or $1/16$;
- $(\gamma_L, \gamma_R) = (1.5, 3)$, for $\rho_R/\rho_L^u = 1.1$;
- $(\gamma_L, \gamma_R) = (3, 1.5)$, for $\rho_R/\rho_L^u = 0.91$.

For such configurations, numerical growth rates were found to be quite sensitive (up to 40% of discrepancy) with respect to the second-order scheme used. In particular, differences in the basic flow numerical results have been observed under the form of more or less pronounced "wall-heating" effects about the interface. Indeed, if a Lagrangian description of the flow ensures that material interfaces are sharply resolved, Godunov-type schemes in Lagrangian coordinates are known to over-predict temperatures at shocked contact discontinuities. The corresponding errors, on the basic flow density and temperature values, which may be modified – but not suppressed – by the method chosen for achieving second order accuracy, are not, of course, without consequences for the linearized flow results. In that respect, we cannot state at this point which of the second order schemes of Section 3.3 should be preferably used. However, in connection with these wall-heating errors, we have found that some flux or slope limiting was necessary for the linearized flow second order schemes to produce, in all circumstances, reliable results with the discrete initial conditions (39).

Let us mention that the aforementioned sensitivity of the computed growth rates is less pronounced (i.e. with discrepancies about 10% or less) for discrete initial conditions which are "smoother" than (39). However when considering initial conditions $(\hat{x}_0, \hat{\Theta}_0)$ with compact supports spanning several computa-

Table 1
Comparison of normalized growth rates obtained with the impulsive model of Vandenboomgaerde et al. [34], the linear theory of Yang et al. [35] and the second order schemes developed in this paper using 500 cells per unit of transverse wavelength

γ_L/γ_R	s	ρ_R/ρ_L^u				
		1.1	2	4	8	16
1.1/1.1	1	*0.023*	*0.150*	*0.252*	*0.303*	*0.32*
		0.004	0.031	0.064	0.094	0.11
	[a]	**0.004**	**0.033**	**0.072**	**0.111**	**0.15**
	0.5	*0.017*	*0.104*	*0.16*	*0.17*	*0.15*
		0.015	0.093	0.14	0.15	0.13
		0.015	**0.091**	**0.14**	**0.15**	**0.13**
	0.05	*0.0021*	*0.012*	*0.018*	*0.018*	*0.016*
		0.0021	0.012	0.018	0.018	0.016
		0.0021	**0.012**	**0.018**	**0.018**	**0.016**
3/3	1	*0.017*	*0.103*	*0.16*	*0.17*	*0.15*
		0.014	0.089	0.14	0.16	0.14
	[a]	**0.016**	**0.097**	**0.16**	**0.18**	**0.17**
	0.5	*0.0084*	*0.050*	*0.074*	*0.076*	*0.067*
		0.0081	0.049	0.072	0.075	0.065
		0.0083	**0.049**	**0.072**	**0.075**	**0.067**
	0.05	*0.00078*	*0.0046*	*0.0067*	*0.0068*	*0.0060*
		0.00078	0.0046	0.0067	0.0068	0.0060
		0.00080	**0.0046**	**0.0068**	**0.0070**	**0.0062**
1.5/3	1	*−0.033*	*0.064*	*0.141*	*0.179*	*0.19*
		−0.0038	0.071	0.14	0.19	0.20
	[a]	**−0.019**	**0.062**	**0.15**	**0.20**	**0.22**
	0.5	*−0.002*	*0.060*	*0.098*	*0.105*	*0.094*
		0.004	0.064	0.10	0.11	0.095
		0.004	**0.063**	**0.10**	**0.11**	**0.097**
	0.05	*0.00114*	*0.0073*	*0.010*	*0.010*	*0.0089*
		0.0012	0.0073	0.010	0.010	0.0089
		0.0012	**0.0073**	**0.010**	**0.010**	**0.0089**

The reflected wave is a shock wave. In each entry, the *first* value corresponds to the impulsive model [34], the second one to the linear theory [35] and the **third** to our numerical result.

[a] Numerical results are obtained for a shock strength $s = 1–10^{-6}$.

tional cells, linearized flow numerical results – whether obtained with first- or second-order schemes – do depend on the actual definitions of the functions $\hat{x}_0$ and $\hat{\Theta}_0$. This dependency is better illustrated if we focus on the propagation, within the L-fluid, of the incoming shock-wave in the particular case where the material interface Σ is not perturbed. In this case, the initial conditions $(\hat{x}_0, \hat{\Theta}_0)$ are chosen among the solutions to the boundary value problems (C.5) and (C.6) with $\widehat{\phi_S} = 0$. At the continuous level, the solutions to system (18) thus correspond to the basic flow, and this regardless of the values taken by $\hat{x}_0$ and $\hat{\Theta}_0$ within $(\xi_{\min}, \xi_\Sigma)$. Otherwise stated, the corresponding linear Eulerian perturbations are identically zero. However, numerical experiments with non-zero values of the initial conditions $(\hat{x}_0, \hat{\Theta}_0)$ show that the computed linear Lagrangian perturbations are characterized by significant levels of linear Eulerian perturbations. Such errors may affect the shock-interface interaction thus leading to inaccuracies in the description of a subsequent Ritchmyer–Meshkov instability. In the absence of a remedy for this numerical defect, the initial condition definition (39) presents the advantage, over other choices, of alleviating such inaccuracies.

Table 2
Comparison of normalized growth rates obtained with the impulsive model of Vandenboomgaerde et al. [34], with the linear theory of Yang et al. [35] and with the second order schemes developed in this paper using 500 cells per unit of transverse wavelength

γ_L/γ_R	s	ρ_R/ρ_L^u				
		0.91	0.5	0.25	0.125	0.0625
1.1/1.1	1	*−0.0230*	*−0.172*	*−0.33*	*−0.43*	*−0.5*
		−0.0039	−0.025	−0.042	−0.047	−0.044
	[a]	**−0.0037**	**−0.025**	**−0.041**	**−0.058**	**−0.075**
	0.5	*−0.017*	*−0.13*	*−0.26*	*−0.35*	*−0.41*
		−0.016	−0.12	−0.24	−0.33	−0.39
		−0.015	**−0.12**	**−0.24**	**−0.34**	**−0.41**
	0.05	*−0.0021*	*−0.017*	*−0.035*	*−0.051*	*−0.062*
		−0.0021	−0.017	−0.035	−0.051	−0.062
		−0.0020	**−0.017**	**−0.035**	**−0.050**	**−0.062**
3/3	1	*−0.017*	*−0.13*	*−0.25*	*−0.33*	*−0.42*
		−0.014	−0.11	−0.22	−0.31	−0.38
	[a]	**−0.014**	**−0.11**	**−0.22**	**−0.32**	**−0.40**
	0.5	*−0.0086*	*−0.069*	*−0.14*	*−0.20*	*−0.24*
		−0.0085	−0.068	−0.14	−0.19	−0.24
		−0.0080	**−0.067**	**−0.14**	**−0.20**	**−0.24**
	0.05	*−0.00081*	*−0.0065*	*−0.013*	*−0.019*	*−0.024*
		−0.00081	−0.0066	−0.013	−0.019	−0.024
		−0.00076	**−0.0065**	**−0.013**	**−0.019**	**−0.024**
3/1.5	1	*0.04*	*−0.086*	*−0.23*	*−0.35*	*−0.43*
		0.016	−0.073	−0.18	−0.28	−0.36
	[a]	**0.029**	**−0.072**	**−0.18**	**−0.28**	**−0.36**
	0.5	*−0.0001*	*−0.068*	*−0.14*	*−0.20*	*−0.25*
		0.0011	−0.066	−0.14	−0.20	−0.25
		0.0015	**−0.065**	**−0.14**	**−0.21**	**−0.25**
	0.05	*−0.00088*	*−0.0074*	*−0.015*	*−0.021*	*−0.025*
		−0.00088	−0.0074	−0.015	−0.021	−0.025
		−0.00084	**−0.0072**	**−0.014**	**−0.021**	**−0.025**

The reflected wave is a rarefaction wave. In each entry, the *first* value corresponds to the impulsive model [34], the second one to the linear theory [35] and the **third** to our numerical result.

[a] Numerical results are obtained for a shock strength $s = 1–10^{-6}$.

5. Conclusion

The Godunov-type schemes presented here offer rather accurate and robust methods for computing – very efficiently, as compared to 2D/3D calculations – multi-dimensional linear perturbations about 1D planar-symmetric flows. These methods which rely on a Lagrangian perturbation formulation and an approximate Riemann solver, are well suited for handling geometrically perturbed material interfaces separating fluids governed by different equations of state. Moreover, the linearized numerical flux which is at the heart of the linear perturbation schemes is obtained in a straightforward manner, the principles involved being immediately applicable to more sophisticated fluid models with zero entropy flux such as two-temperature plasma equations, ideal magnetohydrodynamics, certain models of radiative hydrodynamics or of elasto-plasticity, etc. The scheme numerical capabilities have been illustrated on the simple, yet demanding, configuration of the Richtmyer–Meshkov instability of a single material interface between two perfect gases. Taking advantage of the efficiency of the proposed methods, we have been able to carry out a systematic comparison of linear instability growth rates, extracted from linear perturbation calculations,

with the linear theory results of [35] where various shock strength, fluid density and adiabatic exponent values were considered. Good overall agreement between these two series of results is found. Sources of slight existing discrepancies have been identified to be: (i) wall-heating effects present in the basic flow computations – essentially noticeable for very strong shock waves – and (ii) current definition of linearized flow discrete initial conditions for a perturbed material interface. Further improvements of the present numerical methods should address these two points and include, eventually, the search for a higher accuracy through the use of higher order schemes. Let us mention that the present schemes, as well as those of [28], have been applied to more complex situations such as the stability of a detonation front [20].

Several open questions, with respect to numerical approximations of linearized flows, will be addressed in future works, in particular the treatment of boundary conditions and an extension to spherically-symmetric basic flows. Let us also note that the present perturbation approach is purely Lagrangian and that an Eulerian equivalent, although raising additional difficulties when handling perturbed material interfaces, would be worth pursuing.

Appendix A. Properties of linear Lagrangian perturbations

Herein, for the sake of completeness, we recall two classical results of linear Lagrangian perturbations (see [2, Chapter VII, Eqs. (12) and (15)]) along with their derivation using the notations of this paper.

Proposition 1. *The linear Lagrangian perturbation of the Jacobian J of* (5) *is given by the expression*

$$\mathrm{d}^1 J = J^0 \frac{\partial \mathrm{d}^1 x_j}{\partial \xi_k} \mathrm{d}^0 \left(\frac{\partial \xi_k}{\partial x_j} \right). \tag{A.1}$$

Proof. From the definition of the Jacobian J as the determinant (5), we have

$$\mathrm{d}^1 J = \mathrm{d}^1 \left(\det \left(\frac{\partial x_i}{\partial \xi_j} \right) \right) = \mathrm{d}^0 (J_{kl}) \mathrm{d}^1 \left(\frac{\partial x_k}{\partial \xi_l} \right) = \left(\mathrm{d}^0 J \right)_{kl} \frac{\partial \mathrm{d}^1 x_k}{\partial \xi_l},$$

where J_{kl} denotes the cofactor of $\partial x_k / \partial \xi_l$ in the expression of $\det \left(\partial x_i / \partial \xi_j \right)$. Writing down

$$\frac{\partial \mathrm{d}^1 x_k}{\partial \xi_l} = \frac{\partial \mathrm{d}^1 x_k}{\partial \xi_m} \mathrm{d}^0 \left(\frac{\partial \xi_m}{\partial x_n} \right) \frac{\partial \mathrm{d}^0 x_n}{\partial \xi_l},$$

it comes that

$$\mathrm{d}^1 J = \left(\mathrm{d}^0 J \right)_{kl} \frac{\partial \mathrm{d}^0 x_n}{\partial \xi_l} \frac{\partial \mathrm{d}^1 x_k}{\partial \xi_m} \mathrm{d}^0 \left(\frac{\partial \xi_m}{\partial x_n} \right).$$

Since the sum

$$\left(\mathrm{d}^0 J \right)_{kl} \frac{\partial \mathrm{d}^0 x_n}{\partial \xi_l}$$

is zero as soon as $n \neq k$, and since otherwise

$$\left(\mathrm{d}^0 J \right)_{kl} \frac{\partial \mathrm{d}^0 x_k}{\partial \xi_l} = \mathrm{d}^0 J,$$

we obtain (A.1). □

Proposition 2. *For any scalar function $\bar{\varphi}$ of the variables $(\mathbf{x}, t; \varepsilon)$, we have*

$$\mathrm{d}^1\left(\frac{\partial\bar{\varphi}}{\partial x_j}\right) = \left(\frac{\partial \mathrm{d}^1\varphi}{\partial\xi_k} - \frac{\partial\varphi^0}{\partial\xi_m}\mathrm{d}^0\left(\frac{\partial\xi_m}{\partial x_l}\right)\frac{\partial \mathrm{d}^1 x_l}{\partial\xi_k}\right)\mathrm{d}^0\left(\frac{\partial\xi_k}{\partial x_j}\right), \quad 1 \leqslant j \leqslant 3. \tag{A.2}$$

Proof. By considering $\mathrm{d}^1(\cdot)$ applied to the partial derivatives $\partial\varphi/\partial\xi_i$, we may write

$$\mathrm{d}^1\left(\frac{\partial\varphi}{\partial\xi_i}\right) = \frac{\partial \mathrm{d}^1\varphi}{\partial\xi_i} = \mathrm{d}^1\left(\frac{\partial\bar{\varphi}}{\partial x_j}\frac{\partial x_j}{\partial\xi_i}\right) = \mathrm{d}^1\left(\frac{\partial\bar{\varphi}}{\partial x_j}\right)\frac{\partial \mathrm{d}^0 x_j}{\partial\xi_i} + \mathrm{d}^0\left(\frac{\partial\bar{\varphi}}{\partial x_j}\right)\frac{\partial \mathrm{d}^1 x_j}{\partial\xi_i}, \quad 1 \leqslant i \leqslant 3,$$

thus implying that

$$\mathrm{d}^1\left(\frac{\partial\bar{\varphi}}{\partial x_j}\right)\frac{\partial \mathrm{d}^0 x_j}{\partial\xi_i} = \frac{\partial \mathrm{d}^1\varphi}{\partial\xi_i} - \frac{\partial \mathrm{d}^0\varphi}{\partial\xi_k}\mathrm{d}^0\left(\frac{\partial\xi_k}{\partial x_j}\right)\frac{\partial \mathrm{d}^1 x_j}{\partial\xi_i}, \quad 1 \leqslant i \leqslant 3.$$

Since

$$\frac{\partial \mathrm{d}^0 x_j}{\partial\xi_i}\mathrm{d}^0\left(\frac{\partial\xi_i}{\partial x_l}\right) = \delta_{jl}, \quad 1 \leqslant j,\ \ l \leqslant 3,$$

where δ_{jl} is Kronecker's delta symbol, it ensues that

$$\mathrm{d}^1\left(\frac{\partial\bar{\varphi}}{\partial x_j}\right)\frac{\partial \mathrm{d}^0 x_j}{\partial\xi_i}\mathrm{d}^0\left(\frac{\partial\xi_i}{\partial x_l}\right) = \mathrm{d}^1\left(\frac{\partial\bar{\varphi}}{\partial x_l}\right) = \left(\frac{\partial \mathrm{d}^1\varphi}{\partial\xi_i} - \frac{\partial \mathrm{d}^0\varphi}{\partial\xi_k}\mathrm{d}^0\left(\frac{\partial\xi_k}{\partial x_j}\right)\frac{\partial \mathrm{d}^1 x_j}{\partial\xi_i}\right)\mathrm{d}^0\left(\frac{\partial\xi_i}{\partial x_l}\right), \quad 1 \leqslant l \leqslant 3,$$

which is the desired result. □

Appendix B. Linear perturbation equations for 1D planar-symmetric basic motions

Given the definition (see Section 2.2) of the coordinate system (ξ_1, ξ_2, ξ_3), the Jacobian matrix of the mapping $\mathbf{x} \mapsto \boldsymbol{\xi}$ reads, for $\varepsilon = 0$,

$$\left(\mathrm{d}^0\left(\frac{\partial\xi_i}{\partial x_j}\right)\right) = \begin{pmatrix} \frac{1}{\tau^0} & 0 & 0 \\ 0 & 1 & 0 \\ 0 & 0 & 1 \end{pmatrix}.$$

Using this result, the first integral linear perturbation (11) becomes

$$\mathrm{d}^1\tau = \frac{\partial \mathrm{d}^1 x_1}{\partial\xi_1} + \tau^0\nabla_\perp \cdot \mathrm{d}^1\mathbf{x}_\perp, \tag{B.1}$$

while, benefiting from the fact that the basic solution is independent of the variables (ξ_2, ξ_3), the system of linear perturbation conservation laws (12) reduces to

$$\frac{\partial \mathrm{d}^1\mathbf{V}}{\partial t} + \frac{\partial}{\partial\xi_1}\mathrm{d}^1\mathbf{G}_1(\mathbf{V}) + \tau^0\left\{\frac{\partial}{\partial\xi_j}\mathrm{d}^1\mathbf{G}_j(\mathbf{V})\right\}_{j\neq 1} + \frac{\partial}{\partial\xi_1}\mathbf{G}_1(\mathbf{V}^0)\nabla_\perp \cdot \mathrm{d}^1\mathbf{x}_\perp - \left\{\frac{\partial}{\partial\xi_1}\mathbf{G}_j(\mathbf{V}^0)\frac{\partial \mathrm{d}^1 x_1}{\partial\xi_j}\right\}_{j\neq 1} = \mathbf{0}, \tag{B.2}$$

with the notations: $\mathrm{d}^1\mathbf{x}_\perp = \mathrm{d}^1x_2\mathbf{e}_2 + \mathrm{d}^1x_3\mathbf{e}_3$, $\mathrm{d}^1\mathbf{u}_\perp = \mathrm{d}^1u_2\mathbf{e}_2 + \mathrm{d}^1u_3\mathbf{e}_3$, for the transverse linear Lagrangian displacement and velocity fields, and $\nabla_\perp = (\partial_{\xi_2}\ \partial_{\xi_3})^{\mathrm{t}}$ for the transverse gradient operator. Taking into account the expressions (3) and (13) for the flux components $\mathbf{G}_j(\mathbf{V}^0)$ and their linear Lagrangian perturbations, the above system actually reads

$$\frac{\partial \mathrm{d}^1\tau}{\partial t} - \frac{\partial \mathrm{d}^1u_1}{\partial \xi_1} - \tau^0\nabla_\perp\cdot\mathrm{d}^1\mathbf{u}_\perp - \frac{\partial u_1^0}{\partial \xi_1}\nabla_\perp\cdot\mathrm{d}^1\mathbf{x}_\perp = 0, \tag{B.3}$$

$$\frac{\partial \mathrm{d}^1u_1}{\partial t} + \frac{\partial \mathrm{d}^1p}{\partial \xi_1} + \frac{\partial p^0}{\partial \xi_1}\nabla_\perp\cdot\mathrm{d}^1\mathbf{x}_\perp = 0, \tag{B.4}$$

$$\frac{\partial \mathrm{d}^1\mathbf{u}_\perp}{\partial t} + \tau^0\nabla_\perp\mathrm{d}^1p - \frac{\partial p^0}{\partial \xi_1}\nabla_\perp\mathrm{d}^1x_1 = \mathbf{0}, \tag{B.5}$$

$$\frac{\partial \mathrm{d}^1e}{\partial t} + \frac{\partial}{\partial \xi_1}\mathrm{d}^1(pu_1) + \tau^0p^0\nabla_\perp\cdot\mathrm{d}^1\mathbf{u}_\perp + \frac{\partial}{\partial \xi_1}\left(p^0u_1^0\right)\nabla_\perp\cdot\mathrm{d}^1\mathbf{x}_\perp = 0. \tag{B.6}$$

Classically (e.g. see [5]), the formulation of such a system may be simplified upon performing a Helmholtz decomposition of the vector field $\mathrm{d}^1\mathbf{x}_\perp$.

B.1. Helmholtz decomposition of the transverse displacement field

By Helmholtz's theorem (e.g. see [26]) the vector field $\mathrm{d}^1\mathbf{x}_\perp$ may be decomposed as

$$\mathrm{d}^1\mathbf{x}_\perp = \nabla_\perp\times\boldsymbol{\Psi} + \nabla_\perp\Phi,$$

with $\boldsymbol{\Psi} = \Psi_1\mathbf{e}_1$, Ψ_1 being the stream function of the solenoidal part of $\mathrm{d}^1\mathbf{x}_\perp$, and Φ, the displacement potential, solution of the Poisson equation $\nabla_\perp^2\Phi = \nabla_\perp\cdot\mathrm{d}^1\mathbf{x}_\perp$. Eq. (B.5), implies that $\partial\nabla_\perp^2\Psi_1/\partial t$ is constant in time, whence that solenoidal transverse motions are solid rotations about the x_1-axis with angular velocities determined by initial conditions. Consequently, the transverse motion may be reduced to its irrotational part which is entirely determined by $\nabla_\perp\cdot\mathrm{d}^1\mathbf{x}_\perp$. Introducing the new variables

$$\mathrm{d}^1\Theta = \nabla_\perp\cdot\mathrm{d}^1\mathbf{x}_\perp \quad\text{and}\quad \mathrm{d}^1\Omega = \nabla_\perp\cdot\mathrm{d}^1\mathbf{u}_\perp, \tag{B.7}$$

the vector equation (B.5) is replaced by the scalar equation

$$\frac{\partial \mathrm{d}^1\Omega}{\partial t} + \tau^0\nabla_\perp^2\mathrm{d}^1p - \frac{\partial p^0}{\partial \xi_1}\nabla_\perp^2\mathrm{d}^1x_1 = 0. \tag{B.8}$$

With obvious changes in notations, Eqs. (B.3), (B.4), (B.6) and (B.8) form then a system of equations for the unknowns $(\mathrm{d}^1\tau, \mathrm{d}^1u_1, \mathrm{d}^1\Omega, \mathrm{d}^1e)$, while the trajectory equation (10) is replaced by

$$\frac{\partial \mathrm{d}^1x_1}{\partial t} = \mathrm{d}^1u_1, \quad \frac{\partial \mathrm{d}^1\Theta}{\partial t} = \mathrm{d}^1\Omega, \tag{B.9}$$

and the first integral (B.1) expressed in terms of $\mathrm{d}^1\Theta$.

Appendix C. Initial conditions for a perturbed material contact discontinuity

As a particular example of initial conditions for the system of Eqs. (18), we focus on the case of a material contact discontinuity, say Σ, separating two immiscible fluids which are assumed, for the sake of simplicity, to be initially at rest. Without loss of generality we may assume that in the unperturbed configuration – i.e. for $\varepsilon = 0$ – the discontinuity Σ coincides with the planes of equations $x_1 = 0$ and $\xi_1 = 0$ in their respective coordinate system. Identifying the fluid initially located, when $\varepsilon = 0$, within the half-plane $x_1 < 0$ (respectively $x_1 > 0$) by the subscript L (resp. R), we convene that the domains – in the (ξ_1, ξ_2, ξ_3)-space – occupied by the L- and R-fluids are respectively:

$$\mathscr{D}_{\mathrm{L}} = \{\boldsymbol{\xi};\ -\infty < \xi_1 < 0\}, \quad \text{and} \quad \mathscr{D}_{\mathrm{R}} = \{\boldsymbol{\xi};\ 0 < \xi_1 < +\infty\},$$

while the discontinuity Σ coincides with the plane

$$\mathscr{P} = \{\boldsymbol{\xi}; \xi_1 = 0\}. \tag{C.1}$$

We emphasize that by virtue of the principles of Lagrangian perturbations recalled in Section 2.1 the definitions of $\mathscr{D}_{\mathrm{L}}$, $\mathscr{P}$ and $\mathscr{D}_{\mathrm{R}}$ are invariant as (t, ε) spans $(0, T) \times \mathscr{I}_0$.

When considering perturbed initial conditions we require:

1. For any fluid particle, the initial values of the thermodynamical variables τ and $\mathscr{E}$ to be *independent* of the value of ε in $\mathscr{I}_0$.
2. The restriction to $\mathscr{D}_{\mathrm{L}}$ (respectively $\mathscr{D}_{\mathrm{R}}$) of the mapping $\boldsymbol{\xi} \mapsto \mathbf{x}$ to be a diffeomorphism between $\mathscr{D}_{\mathrm{L}}$ (resp. $\mathscr{D}_{\mathrm{R}}$) and its image, say $D_{\mathrm{L}}(\varepsilon)$ (resp. $D_{\mathrm{R}}(\varepsilon)$), whatever ε in $\mathscr{I}_0$.
3. For all ε in $\mathscr{I}_0$, the discontinuity Σ to remain a material contact discontinuity and to be defined – in the cartesian coordinate system – by the surface S of equation

$$x_1 = \varepsilon \phi_S(x_2, x_3), \tag{C.2}$$

where ϕ_S is a function defined in $\mathbb{R}^2$.

From the first of these requirements, we immediately conclude that

$$\left.\begin{array}{l} \hat{\tau}_0(\xi_1) = 0, \\ \hat{\mathscr{E}}_0(\xi_1) = 0, \end{array}\right\} \quad \text{for} - \infty < \xi_1 < 0 \quad \text{and} \quad 0 < \xi_1 < +\infty, \tag{C.3}$$

for all $\mathbf{k}_\perp$ in $\mathbb{R}^2$. This result and requirement 2 hereinabove imply then that the vector field $\mathrm{d}^1\mathbf{x}_0$ is solenoidal in $\mathscr{D}_{\mathrm{L}} \cup \mathscr{D}_{\mathrm{R}}$, or equivalently – in terms of transverse Fourier components – that

$$\frac{\partial \widehat{x_1}_0}{\partial \xi_1} + \tau_0^0 \hat{\Theta}_0 = 0, \tag{C.4}$$

for ξ_1 in $(-\infty, 0) \cup (0, +\infty)$. Given that a priori the sole boundary condition bearing on the field $(\widehat{x_1}_0, \hat{\Theta}_0)$ is $\widehat{x_1}_0(0) = \widehat{\phi_S}$, as deduced from the definitions (C.1) and (C.2) of Σ, we require in addition that $\widehat{x_1}_0$ be vanishing as $|\xi_1| \to +\infty$, and therefore consider the following boundary value problems (BVPs):

Find the pair of functions $(\widehat{x_1}_0, \hat{\Theta}_0) : \xi_1 \in (-\infty, 0) \cup (0, +\infty) \mapsto (\widehat{x_1}_0, \hat{\Theta}_0)(\xi_1) \in \mathbb{R}^2$ solution of

$$\begin{cases} \frac{\partial \widehat{x_1}_0}{\partial \xi_1} + \tau_{0,\mathrm{L}}^0 \hat{\Theta}_0 = 0, & -\infty < \xi_1 < 0, \\ \lim_{\xi_1 \to -\infty} \widehat{x_1}_0 = 0, & \lim_{\xi_1 \to 0^-} \widehat{x_1}_0 = \widehat{\phi_S}, \end{cases} \tag{C.5}$$

and

$$\begin{cases} \frac{\partial \widehat{x_{1}}_{0}}{\partial \xi_1} + \tau^0_{0,\mathrm{R}} \hat{\Theta}_0 = 0, \quad 0 < \xi_1 < +\infty, \\ \lim_{\xi_1 \to 0^+} \widehat{x_{1}}_{0} = \widehat{\phi_S}, \quad \lim_{\xi_1 \to +\infty} \widehat{x_{1}}_{0} = 0. \end{cases} \tag{C.6}$$

We note that we may require $\widehat{x_{1}}_{0}$ and $\hat{\Theta}_0$ to be, respectively, $\mathscr{C}^{k+1}$ and $\mathscr{C}^k$ functions, for some integer $k \geqslant 0$, in $(-\infty, 0) \cup (0, +\infty)$ or even in $\mathbb{R}$. Solutions to such BVPs are not unique unless additional constraints on the field $\mathrm{d}^1\mathbf{x}_0$ are imposed. Hence, for example, requiring $\mathrm{d}^1\mathbf{x}_0$ to be irrotational leads to a unique definition of $(\widehat{x_{1}}_{0}, \hat{\Theta}_0)$, as solutions of Laplace's equation in the intervals $(-\infty, 0)$ and $(0, +\infty)$, with $\widehat{x_{1}}_{0}$ continuous in $\mathbb{R}$ and $\hat{\Theta}_0$ discontinuous across $\xi_1 = 0$. These considerations along with the definitions (C.3) of $\hat{\tau}_0$ and $\hat{\mathscr{E}}_0$ show that initial values of $(\hat{\mathbf{V}}, \hat{\Omega}, \widehat{x_1}, \hat{\Theta})$ corresponding to a geometrically perturbed material contact discontinuity may be chosen here in the *class of functions*.

References

[1] D.J. Benson, Computational methods in Lagrangian and Eulerian hydrocodes, Comp. Meth. Appl. Mech. Eng. 99 (1992) 235–394.

[2] V. Bjerknes, J. Bjerknes, H. Solberg, T. Bergeron, Hydrodynamique physique avec applications à la météorologie dynamique. Presses Universitaires de France, Paris, 1934 (French edition of Physikalische hydrodynamik, Springer, Berlin, 1933).

[3] F. Bouchut, F. James, One-dimensional transport equations with discontinuous coefficients, Nonlinear Anal., TMA 32 (7) (1998) 891–933.

[4] C. Boudesocque-Dubois, J.-M. Clarisse, Investigation of linear perturbation growth in a planar ablation flow, In: Oleg N. Krokhin, Sergey Y. Gus'kov, Yury A. Merkul'ev (Eds.), ECLIM: 27th European Conference on Laser Interaction with Matter, vol. 5228, SPIE, 2003, pp. 172–183.

[5] L. Brun, B. Sitt, Approche lagrangienne du problème des instabilités hydrodynamiques d'une implosionàsymétrie plane ou sphérique, Technical Report CEA-R-5012, CEA, 1979 (in French).

[6] V.Ya. Bukharova, G.A. Grishina, O.M. Zotova, T.G. Ivtchenko, Linearization of the multi-dimensional equations of gas dynamics with heat conduction in Lagrangian variables, VANT, Ser. Met. i progr. chisl. resh. zad. mat. fiziki 2 (4) (1979) 6–11 (in Russian).

[7] J.P. Cox, Theory of stellar pulsation, in: Princeton Series in Astrophysics, Princeton University Press, Princeton, NJ, 1980.

[8] B. Després, Inégalités entropiques pour un solveur de type Lagrange + convection des équations de l'hydrodynamique, Technical Report 2822, CEA, 1997 (in French).

[9] B. Després, Lagrangian systems of conservation laws. Invariance properties of Lagrangian systems of conservation laws. approximate Riemann solvers and the entropy condition, Numer. Math. 89 (2001) 99–134.

[10] J.-M. Dufour, D. Galmiche, B. Sitt, Investigation of hydrodynamic stability of high aspect ratio targets in laser implosion experiments, in: H. Hora, G.H. Miley (Eds.), Laser Interaction and Related Plasma Phenomena, vol. 6, Plenum Publishing Corp, New York, 1984, pp. 709–730.

[11] E. Godlewski, M. Olazabal, P.-A. Raviart, On the linearization of hyperbolic systems of conservation laws. Application to stability, in: Equations aux dérivées partielles et applications, articles dédiés à J.-L. Lions, Gauthier-Villars, Paris, 1998, pp. 549–570.

[12] E. Godlewski, M. Olazabal, P.-A. Raviart, On the linearization of systems of conservation laws for fluids at a material contact discontinuity, J. Math. Pures Appl. 78 (1999) 1013–1042.

[13] E. Godlewski, M. Olazabal, P.-A. Raviart, A Godunov-type method for studying the linearised stability of a flow. Application to the Richtmyer–Meshkov instability, in: E.F. Toro (Ed.), Godunov Methods: Theory and Applications, Kluwer Academic/Plenum Publishers, New York, 2001, pp. 377–397.

[14] E. Godlewski, P.-A. Raviart, The linearized stability of solutions of nonlinear hyperbolic systems of conservation laws. A general numerical approach, Math. Comp. Simulation 50 (1999) 77–95.

[15] S.K. Godunov, Difference methods for the numerical calculation of the equations of fluid dynamics, Math. Sb. 47 (1959) 271–306.

[16] V.N. Goncharov, Theory of the ablative Richtmyer–Meshkov instability, Phys. Rev. Lett. 82 (10) (1999) 2091–2094.

[17] G.A. Grishina, Linear approximation method in gas dynamics problem numerical computations, Technical Report 121, USSR Academy of Sciences IAM, 1980 (in Russian).

[18] D.B. Henderson, R.L. Morse, Symmetry of laser-driven implosions, Phys. Rev. Lett. 32 (7) (1974) 355–358.

[19] R.L. Holmes, G. Dimonte, B. Fryxell, M.L. Gittings, J.W. Grove, M. Schneider, D.H. Sharp, A.L. Velikovich, R.P. Weaver, Q. Zhang, Richtmyer–Meshkov instability growth: experiment, simulation and theory, J. Fluid Mech. 389 (1999) 55–79.

[20] S. Jaouen, Étude mathématique et numérique de stabilité pour des modèles hydrodynamiques avec transition de phase, PhD thesis, Université Paris 6, 2001.

[21] P. Lax, B. Wendroff, Systems of conservation laws, Comm. Pure Appl. Math. 13 (1960) 217–237.
[22] P. Ledoux, T. Walraven, Variable stars, in: Handbuch der Physik, Springer, Berlin, 1958, pp. 353–604.
[23] A. Majda, The stability of multi-dimensional shock fronts, Memoirs of the A.M.S. 275, Amer. Math. Soc., Providence, 1983.
[24] R.L. McCrory, R.L. Morse, K.A. Taggart, Growth and saturation of instability of spherical implosions driven by laser or charged particle beams, Nucl. Sci. Eng. 64 (1977) 163–176.
[25] E.E. Meshkov, Instability of the interface of two gases accelerated by a shock wave, Soviet Fluid Dynamics 4 (1969) 101–104.
[26] P.M. Morse, H. Feshbach, Methods of Theoretical Physics, McGraw Hill, New York, 1953.
[27] C.D. Munz, On Godunov-type schemes for Lagrangian gas dynamics, SIAM J. Numer. Anal. 31 (1) (1994) 17–42.
[28] M. Olazabal, Modélisation numérique de problèmes de stabilité linéarisée. Application aux équations de la dynamique des gaz et de la MHD idéale. PhD thesis, Université Paris 6, 1998.
[29] R.D. Richtmyer, Taylor instability in shock acceleration of compressible fluids, Commun. Pure Appli. Math. 13 (1960) 297–319.
[30] R.D. Richtmyer, K.W. Morton, Difference Methods for Initial-value Problems, second ed., Wiley-Interscience, New York, 1967.
[31] J.N. Shiau, E.B. Goldman, C.I. Weng, Linear stability analysis of laser-driven spherical implosions, Phys. Rev. Lett. 32 (7) (1974) 352–355.
[32] C. Shu, S. Osher, Efficient implementation of essentially non-oscillatory shock capturing schemes, J. Comp. Phys. 77 (1988) 439–471.
[33] E.F. Toro, Riemann Solvers and Numerical Methods for Fluid Dynamics: A Practical Introduction, second ed., Springer, Berlin, 1999.
[34] M. Vandenboomgaerde, C. Mügler, S. Gauthier, Impulsive model for the Richtmyer–Meshkov instability, Phys. Rev. E 58 (2) (1998) 1874–1882.
[35] Y. Yang, Q. Zhang, D.H. Sharp, Small amplitude theory of Richtmyer–Meshkov instability, Phys. Fluids 6 (5) (1994) 1856–1873.